hour after the injection, the brain was dissected and sliced into 2 mm thick coronal sections in the exactly same way as above experiment. All sections were put in grass slides and their fluorescence was measured at with in vivo imaging system (IVIS, Xenogen Corp., Alameda, CA).

## REFERENCES


Back, T., 1998. Pathophysiology of the ischemic penumbra—revision of a concept. Cell. Mol. Neurobiol. 18, 621–638.

Cipolla, M.J., McCall, A.L., Lessov, N., Porter, J.M., 1997. Reperfusion decreases myogenic reactivity and alters middle cerebral artery function after focal cerebral ischemia in rats. Stroke 28, 176–180.

Cipolla, M.J., Curry, A.B., 2002. Middle cerebral artery function after stroke: the threshold duration of reperfusion for myogenic activity. Stroke 33, 2094–2099.

Cunningham, L.A., Wetzel, M., Rosenberg, G.A., 2005. Multiple roles for MMPs and TIMPs in cerebral ischemia. Glia 50, 329–339.

Dirnagl, U., Iadecola, C., Moskowitz, M.A., 1999. Pathobiology of ischaemic stroke: an integrated view. Trends Neurosci. 22, 391–397.

Erdo, F., Berzsenyi, P., Andrasi, F., 2005. The AMPA-antagonist talampanel is neuroprotective in rodent models of focal cerebral ischemia. Brain Res. Bull. 66, 43–49.

Huang, J., Upadhyay, U.M., Tamargo, R.J., 2006. Inflammation in stroke and focal cerebral ischemia. Surg. Neurol. 66, 232–245.

Kannan, S., Kolhe, P., Raykova, V., Glibatec, M., Kannan, R.M., Lieh-Lai, M., Bassett, D., 2004. Dynamics of cellular entry and drug delivery by dendritic polymers into human lung epithelial carcinoma cells. J. Biomater. Sci. Polym. Ed. 15, 311–330.

Kato, N., Yanaka, K., Hyodo, K., Homma, K., Nagase, S., Nose, T., 2003. Stable nitroxide Tempol ameliorates brain injury by inhibiting lipid peroxidation in a rat model of transient focal cerebral ischemia. Brain Res. 979, 188–193.

Kontos, H.A., 2001. Oxygen radicals in cerebral ischemia: the 2001 Willis lecture. Stroke 32, 2712–2716.

Lo, E.H., 2008. A new penumbra: transitioning from injury into repair after stroke. Nat. Med. 14, 497–500.

Lopez-Sanchez, C., Martin-Romero, F.J., Sun, F., Luis, L., Samhan-Arias, A.K., Garcia-Martinez, V., Gutierrez-Merino, C., 2007. Blood micromolar concentrations of kaempferol afford protection against ischemia/reperfusion-induced damage in rat brain. Brain Res. 1182, 123–137.

Lukyanov, A.N., Hartner, W.C., Torchilin, V.P., 2004. Increased accumulation of PEG-PE micelles in the area of experimental myocardial infarction in rabbits. J. Control. Release 94, 187–193.

Marler, J.R., Goldstein, L.B., 2003. Medicine. Stroke—tPA and the clinic. Science 301, 1677.

Nagasawa, H., Kogure, K., 1989. Correlation between cerebral blood flow and histologic changes in a new rat model of middle cerebral artery occlusion. Stroke 20, 1037–1043.

Rosenberg, G.A., Estrada, E.Y., Dencoff, J.E., 1998. Matrix metalloproteinases and TIMPs are associated with blood–brain barrier opening after reperfusion in rat brain. Stroke 29, 2189–2195.

Seymour, L.W., Miyamoto, Y., Maeda, H., Brereton, M., Strohalm, J., Ulbrich, K., Duncan, R., 1995. Influence of molecular weight on passive tumour accumulation of a soluble macromolecular drug carrier. Eur. J. Cancer. 31A, 766–770.

Svenson, S., 2009. Dendrimers as versatile platform in drug delivery applications. Eur. J. Pharm. Biopharm. 71, 445–462.

Xu, X.H., Zhang, S.M., Yan, W.M., Li, X.R., Zhang, H.Y., Zheng, X.X., 2006. Development of cerebral infarction, apoptotic cell death and expression of X-chromosome-linked inhibitor of apoptosis protein following focal cerebral ischemia in rats. Life Sci. 78, 704–712.

Yang, G.Y., Betz, A.L., 1994. Reperfusion-induced injury to the blood-brain barrier after middle cerebral artery occlusion in rats. Stroke 25, 1658–1664 discussion 1664-5.

Yang, Y., Estrada, E.Y., Thompson, J.F., Liu, W., Rosenberg, G.A., 2007. Matrix metalloproteinase-mediated disruption of tight junction proteins in cerebral vessels is reversed by synthetic matrix metalloproteinase inhibitor in focal ischemia in rat. J. Cereb. Blood Flow Metab. 27, 697–709.

Yoshida, H., Yanai, H., Namiki, Y., Fukatsu-Sasaki, K., Furutani, N., Tada, N., 2006. Neuroprotective effects of edaravone: a novel free radical scavenger in cerebrovascular injury. CNS Drug Rev. 12, 9–20.

Zhang, Z.G., Zhang, L., Tsang, W., Soltanian-Zadeh, H., Morris, D., Zhang, R., Goussev, A., Powers, C., Yeich, T., Chopp, M., 2002. Correlation of VEGF and angiopoietin expression with disruption of blood–brain barrier and angiogenesis after focal cerebral ischemia. J. Cereb. Blood Flow Metab. 22, 379–392.

Zhu, H.C., Gao, X.Q., Xing, Y., Sun, S.G., Li, H.G., Wang, Y.F., 2004. Inhibition of caspase-3 activation and apoptosis is involved in 3-nitropropionic acid-induced ischemic tolerance to transient focal cerebral ischemia in rats. J. Mol. Neurosci. 24, 299–305.


Please cite this article as: Ishii, T., et al., Accumulation of macromolecules in brain parenchyma in acute phase of cerebral infarction/reperfusion, Brain Res. (2010), doi:10.1016/j.brainres.2010.01.039

Cancer Letters 287 (2010) 165–171

Contents lists available at ScienceDirect

Cancer Letters

journal homepage: www.elsevier.com/locate/canlet

# A novel DDS strategy, "dual-targeting", and its application for antineovascular therapy

Yuki Murase [a], Tomohiro Asai [a], Yasufumi Katanasaka [a], Tomoki Sugiyama [a], Kosuke Shimizu [a], Noriyuki Maeda [b], Naoto Oku [a,*]

[a] Department of Medical Biochemistry and Global COE Program, Graduate School of Pharmaceutical Sciences, University of Shizuoka, 52-1 Yada, Suruga-ku, Shizuoka 422-8526, Japan
[b] Nippon Fine Chemical Co. Ltd., Takasago, Hyogo 676-0074, Japan

ARTICLE INFO

*Article history:*
Received 16 December 2008
Received in revised form 25 March 2009
Accepted 8 June 2009

*Keywords:*
Dual-targeting
Drug delivery system
Liposomes
Active-targeting
Antineovascular therapy
Angiogenesis

ABSTRACT

Dual-targeting liposomes modified with Ala-Pro-Arg-Pro-Gly (APRPG) and Gly-Asn-Gly-Arg-Gly (GNGRG) peptides were developed. They remarkably associated to growing human umbilical vein endothelial cells (HUVECs) compared with single-targeting liposomes modified with APRPG or GNGRG. Doxorubicin (DOX) encapsulated in the dual-targeting liposomes significantly suppressed the growth of HUVECs compared with that in single-targeting liposomes. The dual-targeting liposomes containing DOX strongly suppressed tumor growth in Colon26 NL-17 carcinoma-bearing mice. Confocal microscopic data indicated that this anticancer effect was brought by the association of these liposomes to angiogenic vessels in the tumor. These findings suggest that "dual-targeting" would be a hopeful method for targeting therapies.



## 1. Introduction

Liposomes are known as one of the most effective drug carriers for cancer therapy. In liposomal DDS technologies, polyethylene glycol (PEG)-modified liposomes are well known as useful drug carriers for cancer therapy. PEG-modified liposomes have long-circulating characteristics through avoidance of trapping by a reticuloendothelial system (RES) such as liver and spleen [1,2]. PEG-modified liposomes tend to accumulate in tumor tissues thorough passive targeting since leaky angiogenic vessels brings enhanced permeability and retention (EPR) effect [3,4]. In fact, PEG-modified liposomes containing doxorubicin (DOX) have been used in clinical cancer therapy. On the other hand, active-targeting using liposomes modified with ligands such as antibodies and peptides achieves more selective drug delivery to tumor tissues. These ligands that recognize tumor-associated molecules are conjugated to the head of PEG-chain of liposomes [5,6]. Active-targeting using ligand-modified long-circulating PEG-liposomes would be more effective since these liposomes have great opportunity to meet target tissues during long circulation time. Indeed, cancer treatments with stealth immunoliposomes and transferrin-conjugated PEG-liposomes have been successful in animal models [7–9].

*Abbreviations*: DDS, drug delivery system; APRPG, Ala-Pro-Arg-Pro-Gly; GNGRG, Gly-Asn-Gly-Arg-Gly; ANET, antineovascular therapy; HUVECs, human umbilical vein endothelial cells; DOX, doxorubicin; PEG, polyethylene glycol; RES, reticuloendothelial system; EPR, enhanced permeability and retention; RGD, Arg-Gly-Asp; DSPC, distearoylphosphatidylcholine; EGM-2, endothelial cell growth medium-2; FBS, fetal bovine serum; ANOVA, analysis of variance; PEG-Lip, PEG-modified liposomes; PRP-PEG-Lip, APRPG-modified liposomes; NGR-PEG-Lip, GNGRG-modified liposomes; Dual-PEG-Lip, dual-targeting liposomes; PEG-DOX, DOX encapsulated in PEG-Lip; PRP-PEG-DOX, DOX encapsulated in PRP-PEG-Lip; NGR-PEG-DOX, DOX encapsulated in NGR-PEG-Lip; Dual-PEG-DOX, DOX encapsulated in Dual-PEG-Lip; EGFR, epidermal growth factor receptors; FR, folate receptors.

* Corresponding author. Tel.: +81 54 264 5701; fax: +81 54 264 5705.
*E-mail address:* oku@u-shizuoka-ken.ac.jp (N. Oku).

0304-3835/$ - see front matter © 2009 Elsevier Ireland Ltd. All rights reserved.
doi:10.1016/j.canlet.2009.06.008

Angiogenesis is a critical event for growth and hematogenous metastasis of tumors [10,11]. Therefore, antiangiogenic therapies are promised to suppress both tumor growth and metastasis [12,13]. Antineovascular therapy (ANET), one of antiangiogenic therapies, causes indirect tumor regression through damaging angiogenic vessels, which is achieved by delivering anticancer drugs to them with DDS technologies such as liposomes [14]. ANET could avoid the acquirement of drug resistance resulting from genetic or epigenetic mutation since this therapy targets angiogenic endothelial cells that are genetically stable [13]. The therapeutic effect of anticancer drugs would be amplified by targeting angiogenic cells since a large number of cancer cells are maintained by a relatively few endothelial cells for their survival and growth [15]. Furthermore, ANET is expected to have a broad anticancer spectrum since angiogenic vessels are necessary for all kinds of solid tumors.

We previously performed *in vivo* biopanning of a phage-displayed peptide library using an angiogenesis mouse model to identify a targeting-ligand for angiogenic vessel-specific drug delivery. As a result, Ala-Pro-Arg-Pro-Gly (APRPG) was identified as a novel peptide homing to angiogenic vessels [14,16]. Arap and coworkers injected phage-displayed peptide library into the circulation of human breast carcinoma-bearing mice and identified Asn-Gly-Arg (NGR) and Arg-Gly-Asp (RGD) motif [17]. NGR and RGD peptides motif bind selectively to CD13 (aminopeptidase N) and $\alpha_v\beta_3$ or $\alpha_v\beta_5$ integrins, respectively [18–20]. These peptides such as PRP, NGR and RGD were useful as targeting-ligands of liposomes since modification of liposomes with each of these peptides enhanced anticancer activity of DOX in tumor-bearing mice [21,22]. Until now, these peptides were used for angiogenic vessel-targeting individually and combinational effect of them has not been investigated. In the present study, we proposed a novel active-targeting strategy named "dual-targeting" in which two different kinds of targeting-ligands are modified on drug carriers. We hypothesized that two different ligands on the surface of liposomes might enable to enhance the potential of active-targeting cooperatively. We prepared dual-targeting liposomes modified with both APRPG and GNGRG and investigated the usefulness of them for ANET.

## 2. Materials and methods

### 2.1. Preparation of liposomes

All lipids were the products of Nippon Fine Chemical, Co. Ltd. (Takasago, Hyogo, Japan). Distearoylphosphatidylcholine (DSPC) and cholesterol with DSPE-PEG, DSPE-PEG-APRPG or DSPE-PEG-GNGRG (10:5:1 as a molar ratio), or with DSPE-PEG-APRPG and DSPE-PEG-GNGRG (10:5:0.5:0.5 as a molar ratio) were dissolved in chloroform/methanol, dried under reduced pressure, and stored *in vacuo* for at least 1 h. Liposomes were prepared by hydration of the thin lipid film with PBS, and frozen and thawed for three cycles using liquid nitrogen. Then, the liposomes were sized by extruding thrice through a polycarbonate membrane filter with 100 nm pores. Particle size and ζ-potential of the liposomes diluted with PBS were measured by use of a Zetasizer Nano ZS (MALVERN, Worcestershire UK, USA).

For an association study and a histochemical analysis, $DiIC_{18}$ (Molecular Probes Inc., Eugene, OR, USA) was added to the initial chloroform/methanol solution at a dose of 5 mol% of DSPC. For a biodistribution study, a trace amount of [$^3$H]cholesteryl hexadecyl ether (GE Healthcare UK Ltd., Buckinghamshire, England) was added to the initial solution. For a cell proliferation assay and a therapeutic experiment, DOX-encapsulated liposomes were prepared by a modification of the remote-loading method as described previously [23]. The encapsulation efficiency of DOX into the liposomes was more than 90% throughout the experiment. The concentration of DOX was determined by an absorbance at 484 nm.

### 2.2. Association of liposomes to HUVECs

Human umbilical vein endothelial cells (HUVECs, $2 \times 10^4$ cells/well) were seeded on gelatin-coated 24-well plate and cultured in endothelial cell growth medium-2 (EGM-2, Cambrex Bio Science Walkersville, Walkersville, MD) for 48 h at 37 °C in a 5% $CO_2$ incubator. Then, $DiIC_{18}$-labeled liposomes were added (final 0.05 or 0.1 mM as DSPC concentration) and incubated for 4 h at 37 °C. After washing these cells with ice-cold PBS, they were solubilized in 0.1% sodiumdodecylsulfate-containing 10 mM Tris buffer (pH 7.4). The amount of $DiIC_{18}$-labeled liposomes transferred to HUVECs was fluorometrically determined at an excitation wavelength of 549 nm and an emission wavelength of 592 nm by Infinite M200 (Tecan, Grödig, Austria). The amount of proteins in the samples was determined by bicinchoninic acid (BCA) protein assay (Pierce Chemical, IL). The amount of liposomes transferred into HUVECs was corrected by the amount of cellular proteins.

### 2.3. Cell proliferation assay

HUVECs ($5 \times 10^3$ cells/well) were seeded on gelatin-coated 96-well plate and cultured in EGM-2 overnight at 37 °C in a 5% $CO_2$ incubator. Then, DOX or DOX-encapsulated liposomes were added (final 10 μg/ml as a dose of DOX) and incubated for 30 min at 37 °C. After washing these cells with PBS, they were cultured in EGM-2 for 48 h. Then, the growth of these cells was evaluated by a modified MTT assay using TetraColor One™ (Seikagaku, Tokyo, Japan).

### 2.4. Biodistribution study

Colon26 NL-17 cells were cultured in DME/Ham's F12 medium (WAKO, Osaka, Japan) supplemented with streptomycin (100 μg/ml), penicillin (100 units/ml), and 10% fetal bovine serum (FBS) at 37 °C in 5% $CO_2$. After harvesting of these cells, $1.0 \times 10^6$ cells were implanted subcutaneously into the posterior flank of 4-week-old BALB/c male mice (Japan SLC Inc., Shizuoka, Japan). The biodistribution study was performed at day 11 after tumor implantation. Size-matched Colon26 NL-17-bearing mice ($n = 5$) were injected with the radiolabeled liposomes *via* a tail vein (74 kBq/mouse). Twenty-four hours after the injection, the mice

were sacrificed under deep anesthesia for collection of the blood. The plasma was obtained by centrifugation (600g for 5 min). Then the heart, lung, liver, spleen, kidney and tumor were removed, washed with saline, and weighed. The radioactivity in each organ was determined with a liquid scintillation counter (Aloka LSC-3100). Distribution data are presented as % dose per 100 mg tissue. The total amount in the plasma was calculated based on the body weight of mice, where the plasma volume was assumed to be 4.27% of the body weight based on the data of total blood volume [23]. The animals were cared for according to the animal facility guidelines of the University of Shizuoka.

### 2.5. Intratumoral localization of liposomes

Colon26 NL-17 cells ($1.0 \times 10^6$ cells/mouse) were inoculated as described above. DiI-labeled liposomes were administered *via* a tail vein of the mice at 10 days after tumor implantation. At 3 h after injection of the liposomes, the mice were sacrificed under deep anesthesia, and the tumors were dissected. The tumor tissues were embedded in optimal cutting temperature compound (Sakura Finetech, Co. Ltd., Tokyo, Japan) and frozen at −80 °C. Tumor sections (10 μm) were prepared with cryostat microtome (HM 505E, Microm, Walldorf, Germany), mounted on MAS-coated slides (Matsunami Glass Ind., Ltd., Japan), air-dried for 1 h, and washed twice with PBS. Endogenous avidin activity was blocked with a blocking reagent kit (Vector Laboratories, CA). After these sections had been blocked with 1% BSA in PBS, they were incubated with biotinylated anti-mouse CD31 rat monoclonal antibody (Becton Dickinson Lab., Franklin Lakes, NJ) for 18 h at 4 °C and then visualized after incubation with streptavidin-Alexa fluor 488 conjugates (Molecular Probes Inc., Eugene, OR) for 30 min at room temperature in a humid chamber. Then, the sections were mounted with Perma Fluor Aqueous Mounting Medium (Thermo Shandon, PA) and fluorescently observed with the LSM 510 META confocal microscope (Carl Zeiss, Co. Ltd., Germany).

### 2.6. Therapeutic experiment

Colon26 NL-17 cells ($1.0 \times 10^6$ cells/mouse) were inoculated as described above. DOX-encapsulated liposomes or PBS were administered intravenously into the tumor-bearing mice ($n = 5$) at day 8, 11, 14 and 17 after the tumor inoculation. The treatment was started when the tumor volumes had reached about 0.1 $cm^3$. The injected dose of DOX in each administration was 3 mg/kg (about 0.05 mmol/kg as a dose of DSPC in liposomal formulations). The size of the tumors and the body weight of each mouse were monitored. Two bisecting diameters of each tumor were measured with slide calipers to determine the tumor volume. Calculation of the tumor volume was performed using the formula $0.4 \times (a \times b^2)$, where $a$ is the largest and $b$ is the smallest diameter.

### 2.7. Statistical analysis

Differences in a group were evaluated by an analysis of variance (ANOVA) with the Tukey *post hoc* test.

## 3. Results

### 3.1. Characteristics of dual-targeting liposomes

Particle size and ζ-potential of liposomes were determined. All kinds of liposomes used in the following experiments had the size of 110–150 nm in diameter and slightly negative charges (Table 1).

### 3.2. Affinity of dual-targeting liposomes to proliferative endothelial cells

To investigate whether dual-targeting liposomes (Dual-PEG-Lip) have more potent affinity to angiogenic vessels compared with APRPG-PEG-modified or GNGRG-PEG-modified single-targeting liposomes (PRP-PEG-Lip or NGR-PEG-Lip), the association of dual-targeting liposomes to HUVECs stimulated with proangiogenic cytokines were determined (Fig. 1). As a result, all liposomes modified with targeting-peptides were significantly associated to HUVECs compared with PEG-modified liposomes (PEG-Lip) in a dose dependent manner. Moreover, the association amount of Dual-PEG-Lip to HUVECs was significantly higher than that of PRP-PEG-Lip and NGR-PEG-Lip.

### 3.3. Effect of DOX encapsulated in dual-targeting liposomes on the growth of HUVECs

Anti-proliferative effect of DOX encapsulated in dual-targeting liposomes (Dual-PEG-DOX) on HUVECs was determined (Fig. 2). DOX encapsulated in all targeting-liposomes tested (PRP-PEG-Lip containing DOX, PRP-PEG-DOX; NGR-PEG-Lip containing DOX, NGR-PEG-DOX; and Dual-

**Table 1**
Particle size and ζ-potential of liposomes.

| | Particle size (nm) | ζ-Potential (mV) |
|---|---|---|
| PEG-Lip | 121.6 ± 11.7 | −3.1 ± 0.9 |
| PRP-PEG-Lip | 124.8 ± 21.4 | −3.1 ± 0.6 |
| NGR-PEG-Lip | 122.7 ± 22.4 | −2.3 ± 0.9 |
| Dual-PEG-Lip | 116.2 ± 9.7 | −2.9 ± 0.8 |
| PEG-DOX | 145.7 ± 16.2 | −1.2 ± 0.6 |
| PRP-PEG-DOX | 143.7 ± 28.4 | −2.0 ± 0.3 |
| NGR-PEG-DOX | 145.0 ± 44.4 | −2.0 ± 0.3 |
| Dual-PEG-DOX | 136.7 ± 34.0 | −2.8 ± 1.6 |

Parameters represent the mean ± SD.

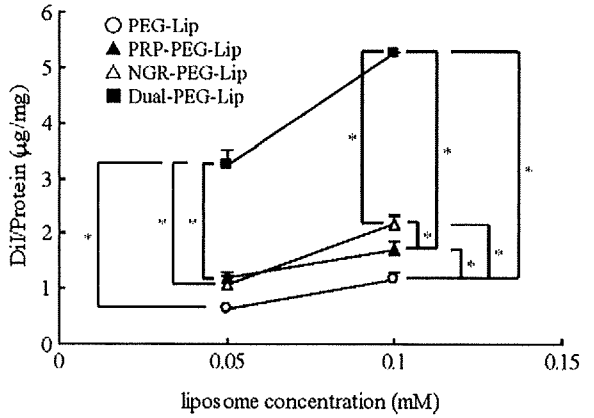


**Fig. 1.** The association of Dual-PEG-Lip to proliferating HUVECs. HUVECs were cultured in EGM-2 for 48 h, then added the indicated dose of $DiIC_{18}$-labeled liposomes and incubated for 4 h at 37 °C. After washing, the amount of liposomes associated to HUVECs was determined fluorometrically. Liposomes associated to HUVECs were represented as amount of $DiIC_{18}$ per cellular protein amount. Open circles, PEG-Lip; closed triangles, PRP-PEG-Lip; open triangles, NGR-PEG-Lip; and closed squares, Dual-PEG-Lip. Data show the mean value and SD. Significant differences are shown with asterisks ($^*P < 0.01$).

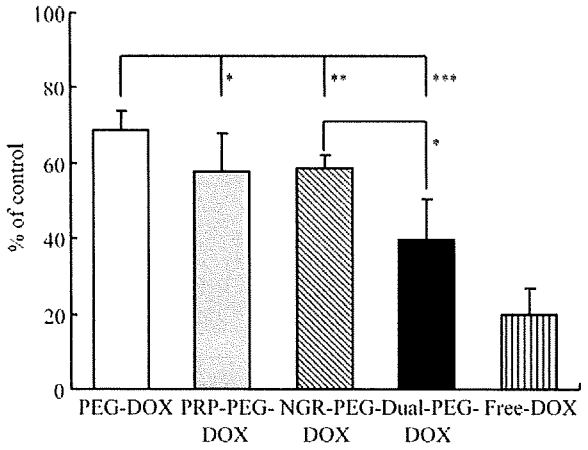


**Fig. 2.** Anti-proliferative effect of Dual-PEG-DOX on proliferating HUVECs. HUVECs were cultured in EGM-2 overnight. Then, DOX or DOX encapsulated in the liposomes were added (final concentration of 10 μg/ml as a DOX dosage) and incubated for 30 min at 37 °C. After 48 h incubation, cell growth was determined by modified MTT assay using TetraColor One™. Data represent the anti-proliferative effects of each sample as percent of control and SD. Open bar, PEG-DOX; grey bar, PRP-PEG-DOX; hatched bar, NGR-PEG-DOX; closed bar, Dual-PEG-DOX; and stripe bar, Free-DOX. Asterisks indicate the significant differences: $^{*}P < 0.05$, $^{**}P < 0.01$ and $^{***}P < 0.001$.

PEG-DOX) significantly suppressed the growth of HUVECs compared with DOX encapsulated in PEG-Lip (PEG-DOX). Furthermore, the antiproliferative effect of Dual-PEG-DOX was significantly higher than that of NGR-PEG-DOX and tended to be high compared with that of PRP-PEG-DOX. These anti-proliferative effects were observed in a dose dependent manner (Supplemental data).

### 3.4. Biodistribution of dual-targeting liposomes

The biodistribution of the liposomes was determined in Colon26 NL-17 carcinoma-bearing mice (Fig. 3). NGR-PEG-Lip tended to accumulate in the spleen. In contrast, the accumulation of PRP-PEG-Lip in the spleen

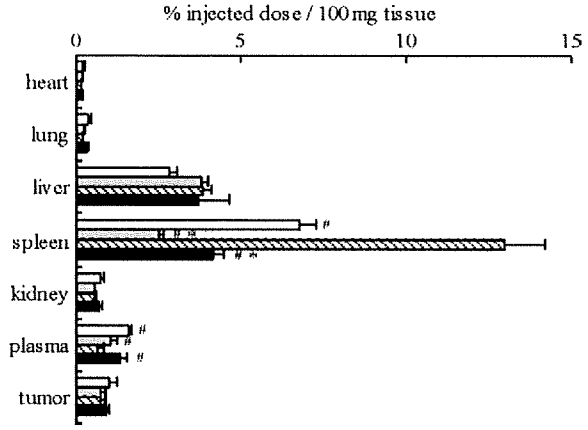


**Fig. 3.** Biodistribution of Dual-PEG-Lip in the tumor-bearing mice. Size-matched Colon26 NL-17-bearing mice ($n = 5$) were injected with radio-labeled liposomes *via* a tail vein. Twenty-four hours after injection, the radioactivity in each organ was determined. Data are presented as percent of the injected dose per 100 mg tissue and SD. Open bar, PEG-Lip; grey bar, PRP-PEG-Lip; hatched bar, NGR-PEG-Lip; and closed bar, Dual-PEG-Lip. Significant differences are shown with asterisks (versus PEG-Lip): $^{*}P < 0.01$, and sharps (versus NGR-PEG-Lip): $^{\#}P < 0.01$.

was lower than PEG-Lip. Interestingly, Dual-PEG-Lip did not accumulate in the spleen although it contains a half amount of GNGRG peptides in comparison to NGR-PEG-Lip. The amount of NGR-PEG-Lip in the plasma was significantly lower than other liposomes tested. On the other hand, Dual-PEG-Lip showed a long-circulating property like PEG-Lip and PRP-PEG-Lip. The accumulation in the tumor was similar level among all liposomes tested.

### 3.5. Intratumoral localization of dual-targeting liposomes

Intratumoral localization of the liposomes was determined in the tumor syngrafts to evaluate the affinity of Dual-PEG-Lip to angiogenic vessels *in vivo* (Fig. 4). As shown in Fig. 4a–c, PEG-Lip was observed around tumor angiogenic vessels, indicating that it extravasated from these vessels. On the other hand, PRP-PEG-Lip (Fig. 4d–f), NGR-PEG-Lip (Fig. 4g–i) and Dual-PEG-Lip (Fig. 4j–l) localized on angiogenic vessels. In addition, Dual-PEG-Lip localized on angiogenic vessels more intensely than PRP-PEG-Lip and NGR-PEG-Lip.

### 3.6. Therapeutic effect of DOX encapsulated in dual-targeting liposomes

The therapeutic effect of Dual-PEG-DOX against the solid tumor was examined (Fig. 5). The body weight change was not observed in all groups tested (data not shown). As shown in the figure, significant differences in the tumor volume were observed between liposomal DOX-treated group (PEG-DOX, PRP-PEG-DOX, NGR-PEG-DOX or Dual-PEG-DOX) and control group 24 days after tumor implantation. Antitumor effect of Dual-PEG-DOX was the highest among all liposomal formulations. Dual-PEG-DOX significantly suppressed the tumor growth in comparison to PEG-DOX.

## 4. Discussion

In the present study, we proposed a novel targeting strategy, "dual-targeting", and applied it to ANET. We firstly determined the affinity of liposomes modified with two different targeting peptides (namely APRPG and GNGRG) to proliferating HUVECs as an *in vitro* model of angiogenic endothelial cells. As a result, Dual-PEG-Lip showed the highest affinity to proliferating HUVECs dose-dependently. This data suggests that two different kinds of angiogenic vessel-targeting peptides on the liposomal surface cooperatively enhanced the association of these liposomes to proliferating HUVECs. Saul et al. previously reported that liposomes targeting epidermal growth factor receptors (EGFR) and folate receptors (FR) improved selectivity to target cells compared with single-ligand liposomes [24]. Although these liposomes attenuated non-specific binding to non-target cells, the affinity of them to target cells was not determined. In contrast, our data provided the evidence that dual-targeting achieved enhancement of the targeting activity. In fact, Dual-PEG-DOX suppressed the growth of proliferating HUVECs in comparison to non-targeting or single-targeting liposomal DOX, reflecting that Dual-PEG-Lip showed the highest affinity to proliferating HUVECs.

Previous study showed that liposomes modified with NGR accumulated in the spleen after intravenous injection [22]. Our data also indicated that NGR-PEG-Lip tended to accumulate in the spleen. However, this wrong property caused by NGR was improved in Dual-PEG-Lip administration group. Consequently, Dual-PEG-Lip remained in the plasma more than NGR-PEG-Lip. These results might be related to the amount of peptide on the liposome surface although precise mechanism is not cleared at present. There were no statistical differences in the accumulation

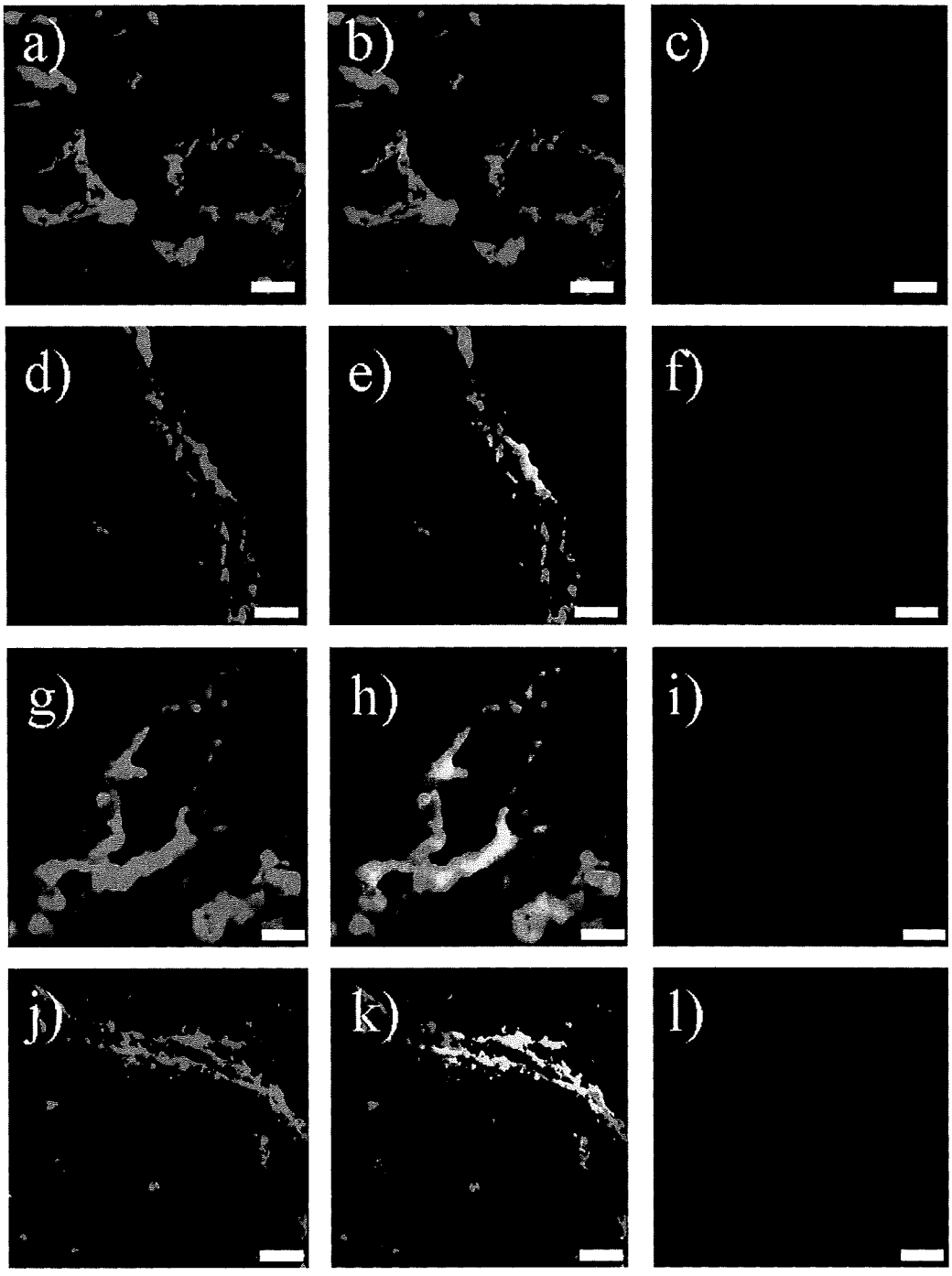


**Fig. 4.** Localization of Dual-PEG-Lip in the tumor. Colon26 NL-17-bearing mice were intravenously injected with PEG-Lip (a–c), PRP-PEG-Lip (d–f), NGR-PEG-Lip (g–i) or Dual-PEG-Lip (j–l) labeled with $DiIC_{18}$ at day 10 after tumor implantation. At 3 h after injection, the tumors were dissected, and then frozen-sections (10 μm) were prepared. Immunofluorescence staining for CD31 was performed to visualize endothelial cells. Green images indicate CD31-positive regions (a, d, g and j), and red images show liposomal distribution (c, f, i and l). Panels b, e, h and k represent the merged images of them. Yellow portions indicate the localization of liposomes at the site of vascular endothelial cells. Scale bars represent 20 μm.

of liposomes to tumor tissue. However, intratumoral distribution of Dual-PEG-Lip in Colon26 NL-17-bearing mice was obviously different. The results showed that targeting liposomes bound to angiogenic vessels whereas PEG-Lip did not. Moreover, Dual-PEG-Lip showed further enhanced targeting activity to angiogenic vessels in comparison to PRP-PEG-Lip or NGR-PEG-Lip along with the result from the *in vitro* association experiment. Thus, the association

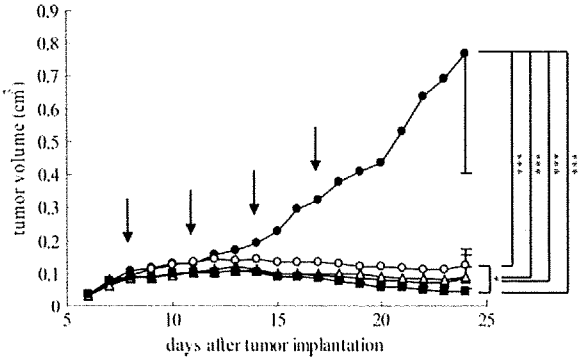


**Fig. 5.** Therapeutic effect of Dual-PEG-DOX in tumor-bearing mice. Colon26 NL-17-bearing mice ($n = 5$) were intravenously injected with PBS (closed circles), PEG-DOX (open circles), PRP-PEG-DOX (closed triangles), NGR-PEG-DOX (open triangles) or Dual-PEG-DOX (closed squares) at days 8, 11, 14 and 17 after tumor implantation. Injected dose of liposomal DOX were 3 mg/kg as DOX in each administration. Tumor volume and body weight (data not shown) of tumor-bearing mice were monitored. Data represent the mean tumor volume and SD, where the SD bars are shown only for the last points (day 24). Arrows show the days of injection. Asterisks show the significant differences: $^{*}P < 0.05$ and $^{***}P < 0.001$.

with angiogenic vessels *in vivo* was also improved effectively by use of dual-targeting liposomes. In our previous studies, we demonstrated that DOX encapsulated in angiogenic vessel-targeted liposomes was localized exclusively to angiogenic endothelial cells and damaged them [25]. Finally the therapeutic effect of Dual-PEG-DOX against the solid tumor was examined. Our data showed that Dual-PEG-DOX strongly suppressed the tumor growth compared with other formulations due to their potent targeting ability to angiogenic vessels. The therapeutic effects of Dual-PEG-DOX might be further enhanced by adjusting the amount of DOX in the liposomes. These findings give enough evidences for usefulness of dual-targeting liposomes in ANET.

From the result obtained in this study, it would be expected that "dual-targeting" is a useful targeting strategy for ANET. For example, combination of peptides used here and RGD would be promising approach. In addition, the investigation about the rate of peptides on dual-targeting liposomal surface would be interesting since we modified an equal amount of APRPG and GNGRG as a tentative rate. The most notable finding presented here is the fact that the targeting ability of liposomes was enhanced by dual-targeting. Dual-targeting would be available for a number of targeting therapies because most of target organs express multiple address molecules.

## Conflicts of interest

None declared.

## Acknowledgement

This research was supported by Grant-in-Aid for Scientific Research on Priority Areas.

## Appendix A. Supplementary material

Supplementary data associated with this article can be found, in the online version, at doi:10.1016/j.canlet.2009.06.008.

## References

[1] T. Sakakibara, F.A. Chen, H. Kida, K. Kunieda, R.E. Cuenca, F.J. Martin, R.B. Bankert, Doxorubicin encapsulated in sterically stabilized liposomes is superior to free drug or drug-containing conventional liposomes at suppressing growth and metastases of human lung tumor xenografts, Cancer Res. 56 (1996) 3743–3746.
[2] D.D. Lasic, Doxorubicin in sterically stabilized liposomes, Nature 380 (1996) 561–562.
[3] Y. Matsumura, H. Maeda, A new concept for macromolecular therapeutics in cancer chemotherapy: mechanism of tumoritropic accumulation of proteins and the antitumor agent smancs, Cancer Res. 46 (1986) 6387–6392.
[4] F.M. Muggia, Doxorubicin-polymer conjugates: further demonstration of the concept of enhanced permeability and retention, Clin. Cancer Res. 5 (1999) 7–8.
[5] J.W. Park, K. Hong, D.B. Kirpotin, O. Meyer, D. Papahadjopoulos, C.C. Benz, Anti-HER2 immunoliposomes for targeted therapy of human tumors, Cancer Lett. 118 (1997) 153–160.
[6] X.B. Xiong, Y. Huang, W.L. Lu, X. Zhang, H. Zhang, T. Nagai, Q. Zhang, Intracellular delivery of doxorubicin with RGD-modified sterically stabilized liposomes for an improved antitumor efficacy: in vitro and in vivo, J. Pharm. Sci. 94 (2005) 1782–1793.
[7] C. Brignole, D. Marimpietri, C. Gambini, T.M. Allen, M. Ponzoni, F. Pastorino, Development of Fab' fragments of anti-GD(2) immunoliposomes entrapping doxorubicin for experimental therapy of human neuroblastoma, Cancer Lett. 197 (2003) 199–204.
[8] F. Pastorino, C. Brignole, D. Marimpietri, P. Sapra, E.H. Moase, T.M. Allen, M. Ponzoni, Doxorubicin-loaded Fab' fragments of anti-disialoganglioside immunoliposomes selectively inhibit the growth and dissemination of human neuroblastoma in nude mice, Cancer Res. 63 (2003) 86–92.
[9] O. Ishida, K. Maruyama, H. Tanahashi, M. Iwatsuru, K. Sasaki, M. Eriguchi, H. Yanagie, Liposomes bearing polyethyleneglycol-coupled transferrin with intracellular targeting property to the solid tumors in vivo, Pharm. Res. 18 (2001) 1042–1048.
[10] J. Folkman, P.A. D'Amore, Blood vessel formation: what is its molecular basis?, Cell 87 (1996) 1153–1155
[11] M.S. O'Reilly, L. Holmgren, C. Chen, J. Folkman, Angiostatin induces and sustains dormancy of human primary tumors in mice, Nat. Med. 2 (1996) 689–692.
[12] M. Skobe, P. Rockwell, N. Goldstein, S. Vosseler, N.E. Fusenig, Halting angiogenesis suppresses carcinoma cell invasion, Nat. Med. 3 (1997) 1222–1227.
[13] T. Browder, C.E. Butterfield, B.M. Kraling, B. Shi, B. Marshall, M.S. O'Reilly, J. Folkman, Antiangiogenic scheduling of chemotherapy improves efficacy against experimental drug-resistant cancer, Cancer Res. 60 (2000) 1878–1886.
[14] N. Oku, T. Asai, K. Watanabe, K. Kuromi, M. Nagatsuka, K. Kurohane, H. Kikkawa, K. Ogino, M. Tanaka, D. Ishikawa, H. Tsukada, M. Momose, J. Nakayama, T. Taki, Anti-neovascular therapy using novel peptides homing to angiogenic vessels, Oncogene 21 (2002) 2662–2669.
[15] R.K. Jain, Normalizing tumor vasculature with anti-angiogenic therapy: a new paradigm for combination therapy, Nat. Med. 7 (2001) 987–989.
[16] T. Asai, K. Shimizu, M. Kondo, K. Kuromi, K. Watanabe, K. Ogino, T. Taki, S. Shuto, A. Matsuda, N. Oku, Anti-neovascular therapy by liposomal DPP-CNDAC targeted to angiogenic vessels, FEBS Lett. 520 (2002) 167–170.
[17] W. Arap, R. Pasqualini, E. Ruoslahti, Cancer treatment by targeted drug delivery to tumor vasculature in a mouse model, Science 279 (1998) 377–380.
[18] R. Pasqualini, E. Koivunen, R. Kain, J. Lahdenranta, M. Sakamoto, A. Stryhn, R.A. Ashmun, L.H. Shapiro, W. Arap, E. Ruoslahti, Aminopeptidase N is a receptor for tumor-homing peptides and a target for inhibiting angiogenesis, Cancer Res. 60 (2000) 722–727.
[19] E. Ruoslahti, RGD and other recognition sequences for integrins, Annu. Rev. Cell Dev. Biol. 12 (1996) 697–715.

[20] E. Koivunen, B. Wang, E. Ruoslahti, Phage libraries displaying cyclic peptides with different ring sizes: ligand specificities of the RGD-directed integrins, Biotechnology (NY) 13 (1995) 265–270.
[21] N. Maeda, Y. Takeuchi, M. Takada, Y. Sadzuka, Y. Namba, N. Oku, Anti-neovascular therapy by use of tumor neovasculature-targeted long-circulating liposome, J. Control. Release 100 (2004) 41–52.
[22] F. Pastorino, C. Brignole, D. Marimpietri, M. Cilli, C. Gambini, D. Ribatti, R. Longhi, T.M. Allen, A. Corti, M. Ponzoni, Vascular damage and anti-angiogenic effects of tumor vessel-targeted liposomal chemotherapy, Cancer Res. 63 (2003) 7400–7409.
[23] N. Oku, K. Doi, Y. Namba, S. Okada, Therapeutic effect of adriamycin encapsulated in long-circulating liposomes on Meth-A-sarcoma-bearing mice, Int. J. Cancer 58 (1994) 415–419.
[24] J.M. Saul, A.V. Annapragada, R.V. Bellamkonda, A dual-ligand approach for enhancing targeting selectivity of therapeutic nanocarriers, J. Control. Release 114 (2006) 277–287.
[25] K. Shimizu, T. Asai, C. Fuse, Y. Sadzuka, T. Sonobe, K. Ogino, T. Taki, T. Tanaka, N. Oku, Applicability of anti-neovascular therapy to drug-resistant tumor: Suppression of drug-resistant P388 tumor growth with neovessel-targeted liposomal adriamycin, Int. J. Pharm. 296 (2005) 133–141.

Journal of Controlled Release 141 (2010) 208–215

Contents lists available at ScienceDirect

Journal of Controlled Release

journal homepage: www.elsevier.com/locate/jconrel

# Temperature-dependent transfer of amphotericin B from liposomal membrane of AmBisome to fungal cell membrane

Kosuke Shimizu [a], Masaaki Osada [a], Koji Takemoto [b], Yutaka Yamamoto [b], Tomohiro Asai [a], Naoto Oku [a,*]

[a] Department of Medical Biochemistry and Global COE program, School of Pharmaceutical Sciences, University of Shizuoka, 52-1 Yada, Suruga-ku, Shizuoka 422-8526, Japan
[b] Dainippon Sumitomo Pharma Co., Ltd., 1-98 Kasugade Naka 3-Chome, Konohana-ku, Osaka 554-0022, Japan

ARTICLE INFO

*Article history:*
Received 18 April 2009
Accepted 22 September 2009
Available online 6 October 2009

*Keywords:*
AmBisome
Temperature-dependency
Cell wall
Ergosterol
Membrane fluidity

ABSTRACT

Liposomal amphotericin B (AMPH-B), also known as AmBisome, exhibits a potent antifungal effect through its binding to ergosterol contained within the fungal cell membrane. However, the mechanism responsible for the movement of AmBisome-derived AMPH-B to the fungal cell membrane through the cell wall is not yet clear. Therefore, in the present study we aimed at elucidating this mechanism operating in *Saccharomyces cerevisiae*. AmBisome showed its antifungal effect against *S. cerevisiae* at 35 °C but not at 4 °C, whereas free AMPH-B was effective at both temperatures. A significant difference in the amount of AMPH-B transferred to the fungal cells between incubation at 4 and 35 °C was also observed when AmBisome was used. Confocal microscopic study, however, indicated that NBD-labeled AmBisome was localized on the surface of the fungal cells at either temperature. To decrease the affinity of AMPH-B for the liposomal membrane, we entrapped AMPH-B in fluid liposomes containing egg yolk phosphatidylcholine (EPC) instead of hydrogenated soy PC (HSPC). These liposomes showed the antifungal effect even at 4 °C. On the contrary, AMPH-B in liposomes containing ergosterol (Erg-AmB) instead of cholesterol showed a significantly weaker antifungal effect at 35 °C with reduced transfer of AMPH-B to the fungal cells. These results suggest that not the binding of AmBisome to target cells but the transfer of AMPH-B from liposomal membrane of AmBisome to the cell membrane is critical for the antifungal activity of AmBisome. This transfer is dependent on the temperature, fluidity of the liposomal membrane, and the affinity of AMPH-B for the fungal cell membrane.



## 1. Introduction

Since patients with infectious diseases caused by certain bacteria or fungi are at a high risk for death, the development of effective drugs for these diseases is of great importance. Mycosis is an infectious disease caused by fungal invasion, and it is divided into 3 classes based on the infection site. Among them, infection by fungi at deep internal organ such as lung and brain is the most serious and is known as deep mycosis. Amphotericin B (AMPH-B), a drug with strong antifungal activity, is effective against deep mycosis and also has a wide antibacterial spectrum [1,2]. As to its mechanism of action, AMPH-B is known to bind to ergosterol contained in the fungal cell membrane, which binding induces a permeability change in the membrane [3,4]. Since AMPH-B also has the ability to bind to cholesterol to some extent [5], it causes side effects such as nephrotoxicity [6]. In order to reduce the side effects of AMPH-B, a liposomal formulation of AMPH-B, known as AmBisome, has been developed. AmBisome is a small unilamellar vesicle containing AMPH-B that is stably retained in the hydrophobic part of the liposomal membrane by complexing with liposomal cholesterol. Since liposomalization of AMPH-B prolongs the circulation of AMPH-B in the bloodstream and decreases the transfer of AMPH-B to cell-membrane cholesterol, the use of AmBisome reduces the side effects of AMPH-B [7–11]. The mechanism of transfer of AMPH-B from AmBisome to the fungal membrane is still unclear, since AmBisome retains the drug in the liposomal membrane rather tightly. By electron microscopy Adler-Moore et al. previously examined the localization of liposomal lipids of AmBisome after exposure to fungal cells such as *Candida glabrata* and *Aspergillus fumigatus* and observed that AmBisome-derived lipids were distributed throughout the cytoplasm of the fungal cells after long-term incubation [12,13]. They also speculated that AmBisome has an affinity for the fungal cell wall and initially binds to it and that the liposomal lipids from AmBisome become dispersed throughout the cytoplasm after damage to the fungal cell membrane caused by AMPH-B released from disrupted AmBisome [13]. Their report indicates that the transfer of AmBisome-derived AMPH-B to the fungal cell membrane is a key step in the action of AmBisome against fungi.

In the present study, we aimed at elucidating the mechanism underlying the transfer of AMPH-B from AmBisome to the fungal cell membrane by using *Saccharomyces cerevisiae* as a model fungal cell. *S. cerevisiae* has a thick cell wall similar to that of other fungal cells [14].

*Abbreviations:* AMPH-B, amphotericin B; EPC, egg yolk phosphatidylcholine; EPG, egg yolk phosphatidylglycerol; DSPG, distearoylphosphatidylglycerol; HSPC, hydrogenated soy phosphatidylcholine; NBD-PE, *N*-4-nitrobenzo-2-oxa-13-diazol phosphatidylethanolamine.

* Corresponding author. Tel.: +81 54 264 5701; fax: +81 54 264 5705.
*E-mail address:* oku@u-shizuoka-ken.ac.jp (N. Oku).

0168-3659/$ – see front matter © 2009 Elsevier B.V. All rights reserved.
doi:10.1016/j.jconrel.2009.09.019

At first, we examined the temperature dependence of AmBisome activity against *S. cerevisiae*, and observed that, unlike AMPH-B, the antifungal activity of AmBisome was drastically suppressed at a low temperature. Then, we examined the localization of AmBisome in yeast cells at different temperatures by confocal laser-scanning microscopy and measured the amount of AMPH-B taken up into the cells. The transfer of AMPH-B from AmBisome to the cell and the antifungal activity of the liposomes were increased by raising the incubation temperature. Interestingly, AMPH-B in a fluid liposomal membrane was taken up into the cells more easily and was fungicidal at a low temperature. On the contrary, AMPH-B in ergosterol-containing liposomes was taken up into the cells in less amount; and the cytotoxic action was suppressed even at a high temperature. The results indicate the importance of translocation of AMPH-B from AmBisome to the cells in its antifungal activity.

## 2. Materials and methods

### 2.1. Reagents

AmBisome was the product of Dainippon Sumitomo Pharma Co., Ltd. (Osaka, Japan) Hydrogenated soy phosphatidylcholine (HSPC), distearoylphosphatidylglycerol (DSPG), egg yolk phosphatidylcholine (EPC), egg yolk phosphatidylglycerol (EPG), and cholesterol were gifts from Nippon Fine Chemical Co., Ltd. (Hyogo, Japan). Amphotericin B (AMPH-B), ergosterol, and *N*-4-nitrobenzo-2-oxa-13-diazol phosphatidylethanolamine (NBD-PE) were purchased from The United States Pharmacopeial Convention, Inc. (Rockville, MD, U.S.A.), Sigma-Aldrich Co. (St Louis, MO, U.S.A.), and Avanti Polar Lipids, Inc. (Alabaster, AL, U.S.A.), respectively. Rhodamine-dextran (10 kDa) was purchased from Wako Pure Chemical Industries, Ltd.

### 2.2. Yeast cell culture

Yeast cells of the *S. cerevisiae* ATCC 9763 (ATCC, U.S.A.) were used as a model of fungal cells in this experiment. They were colonized on YPD/agar medium and kept at 4 °C. Before experimental use, a single colony was picked up and grown in YPD medium with shaking at 30 °C for at least 12 h; and the $OD_{600}$ of the cell suspension was adjusted to 0.1 using RPMI 1640 medium (Sigma-Aldrich Co.) buffered to pH 7.0 with 0.165 M MOPS (Dojindo Laboratories, Kumamoto, Japan).

### 2.3. Preparation of liposomes

AmBisome (liposomal AMPH-B) was composed of HSPC, DSPG, cholesterol, and AMPH-B (10:4:5:2 as a molar ratio). AmBisome solution was prepared by hydration of lyophilized AmBisomal components with ultrapure water. For preparation of NBD-labeled AmBisome, the lyophilized AmBisomal components were firstly dissolved in chloroform, after which NBD-PE solution was added to them. Then, they were lyophilized again with *t*-butanol and rehydrated with succinate-buffered solution (pH 5.5). Unincorporated NBD-PE was removed by gel filtration chromatography with a PD-10 column. For preparation of AmBisome encapsulating rhodamine-dextran, the lyophilized AmBisomal components were hydrated with rhodamine-dextran solution; and then free rhodamine-dextran was removed by column chromatography with Sepharose™ 4 Fast Flow (GE Healthcare UK Ltd., England). AMPH-B in liposomes containing ergosterol (Erg-AmB) was prepared with HSPC, DSPG, ergosterol, and AMPH-B (10:4:5:2 as a molar ratio). The thin lipid film containing AMPH-B was hydrated with succinate-buffered solution with 9% sucrose at 60 °C and freeze-thawed with liquid nitrogen for 3 cycles. The obtained liposomal solution was sized by sonication. Unincorporated AMPH-B was removed by column chromatography with Sepharose™ 4 Fast Flow. Liposomal AMPH-B composed of highly fluid phospholipids (Egg-AmB) was prepared with EPC, EPG, cholesterol, and AMPH-B (10:4:5:2 as a molar ratio) in the similar manner as used to prepare Erg-AmB. The particle size of each liposome was measured by dynamic light scattering analysis with a Zetasizer Nano (Malvern Instruments, Malvern, U.K.) and was about 100 nm in diameter.

### 2.4. Colony formation assay

Each liposomal AMPH-B diluted in succinate-buffered solution with 9% sucrose or free AMPH-B dissolved in 0.1% DMSO (final conc.) at a concentration of 20 μM as AMPH-B was added to a yeast cell suspension and incubated in MOPS-buffered RPMI 1640 medium at 4 or 35 °C for 0.5 or 3 h. Then, the cell suspension was centrifuged and washed twice with PBS. The cell pellet was resuspended in PBS and plated on YPD/agar medium. After 24 h of incubation at 30 °C, the number of colonies formed was counted.

### 2.5. Confocal microscopy

NBD-labeled liposomal AMPH-B (20 μM) was added to a yeast cell suspension, which was then incubated in MOPS-buffered RPMI 1640 medium at 4 or 35 °C for 3 or 24 h with shaking. After having been washed 3 times with PBS, the cells were fixed with 4% paraformaldehyde and stained with Fluorescent Brightener 28 (Sigma-Aldrich Co., U.S.A.) for cell-wall imaging. After another 3 washes with PBS, the cells were attached to MAS-coated glass slides (Matsunami Glass Ind., Ltd., Japan) by centrifugation, and then localization of liposomes in yeast cells was observed under an LSM510 META confocal laser-scanning microscope (Carl Zeiss, Inc., Germany).

### 2.6. Measurement of the amount of AMPH-B transferred to yeast cells

Liposomal AMPH-B (20 μM) was added to a yeast cell suspension, which was then incubated in MOPS-buffered RPMI 1640 medium with shaking at 4 or 35 °C for 0.5 or 3 h. After having been washed with PBS, the cells were disrupted by using glass beads with shaking and sonication, and AMPH-B in the cells was extracted with methanol. After centrifugation, the methanol extract was evaporated; and the residual AMPH-B was dissolved in the mobile phase for HPLC analysis. The HPLC conditions were the following: Column, TSKgel ODS-100Z 4.6×250 mm (Tosoh Co., Japan); mobile phase, acetonitrile and 2.5 mM EDTA (pH 5.0), 4:6 (v/v); temperature, 35 °C; injection volume, 50 μL; flow rate, 1.0 mL/min; and UV detection, 405 nm. Smart Chrom software was used for control of the HPLC system and data processing.

In the inhibition experiment, AmBisome was added to a yeast cell suspension, which was subsequently incubated in the presence or absence of drug free cholesterol liposomes (Cho-Lip) or vacant ergosterol liposomes (Erg-Lip) in MOPS-buffered RPMI 1640 medium. After a 3-h incubation, the amount of AMPH-B transferred to the cells was measured.

### 2.7. Investigation of AmBisome disruption

Rhodamine-encapsulating AmBisome was added to different numbers of yeast cells ($OD_{600}$ = 0.1 or 0.3), and the cells were incubated in MOPS-buffered RPMI 1640 medium for 0.5 or 3 h at 4 or 35 °C. After centrifugation for washing, the supernatant medium was collected and ultracentrifuged to separate the intact AmBisome into the pellet. The resulting supernatant was then collected, and the fluorescence intensity of the rhodamine-dextran that had been released into the medium from AmBisome was measured.

### 2.8. FRAP experiment

NBD-labeled AmBisome and Egg-AmB were similarly prepared as described above and then gradually frozen to make giant-sized liposomes. Then, these liposomes were applied on MAS-coated slide glasses and dried in the dark at room temperature for overnight. FRAP experiments were performed with LSM510 META confocal laser-

scanning microscope according to the protocol of LSM510 for FRAP experiment.

### 2.9. Statistic analysis

The variance in a group was evaluated by use of the *F*-test, and the differences among the groups were evaluated by using Student's *t*-test.

## 3. Results

### 3.1. Temperature-dependent antifungal activity of AmBisome against S. cerevisiae

To confirm the temperature dependence of AmBisome antifungal activity, we evaluated the effect of AmBisome against *S. cerevisiae* at 4 or 35 °C by using the colony formation assay. As shown Fig. 1A, AmBisome showed time-dependent antifungal activity against yeast cells at 35 °C. Free AMPH-B showed stronger antifungal activity than AmBisome, and no colonies were found even after just 0.5 h of incubation with it at 35 °C. On the other hand, the antifungal effect of AmBisome was significantly reduced at 4 °C incubation (Fig. 1B), and the number of colonies was quite similar to that of the control, suggesting the antifungal effect of AmBisome to be temperature-dependent. In contrast, free AMPH-B showed strong fungicidal activity even at this temperature. These results are summarized in Fig. 1C.

### 3.2. Binding of AmBisome to the surface of yeast cells

In general, intact liposome is unable to pass through the fungal cell wall due to its particle size. However, the cell wall penetration of AmBisome has not been fully elucidated, and it is not clear when or where AmBisome-derived AMPH-B is transferred to the fungal cell membrane. To elucidate the mechanism, we prepared NBD-labeled AmBisome and used confocal laser-scanning microscopy to observe its localization in yeast cells after exposure. AmBisome was observed to bind to the surface of yeast cells after a 3-h exposure at 35 °C (Fig. 2A). Especially, AmBisome often bound to budding or interface site of yeast cells. Furthermore, AmBisome-derived fluorescence was observed in the cytoplasm after 24 h of incubation at this temperature (Fig. 2B). Although liposomes without encapsulated AMPH-B also bound to the cell surface, they were not incorporated into the cytoplasm after a 24-h incubation (data not shown). On the other hand, similar to the 35 °C incubation, AmBisome bound to the cell surface after a 3-h incubation at 4 °C (Fig. 2A). However, unlike that at 35 °C, AmBisome-derived fluorescence was present only on the cell surface after 24 h of incubation at the lower temperature (Fig. 2B). The cellular uptake of AmBisome after 24 h incubation at 35 °C, would be the result of permeability increase in cell membrane caused by AMPH-B transferred to the membrane, since the distribution of NBD-labeled AmBisome in *S. cerevisiae* in the presence of free AMPH-B at 4 °C, NBD-labeled AmBisome was observed in the cytosol (data not shown).

### 3.3. Temperature-dependent transfer of AMPH-B from AmBisome to yeast cells

Next, we compared the amount of AMPH-B transferred to yeast cells at different incubation temperatures. AmBisome was added to the yeast cell suspension, and the cells were incubated at 4 or 35 °C. Thereafter, the amount of AMPH-B transferred to the cells was determined by HPLC. As a result, the amount of AMPH-B in the yeast cells was reduced at 4 °C of incubation (Fig. 3), suggesting that this transfer mechanism of AMPH-B from AmBisome is temperature-dependent.

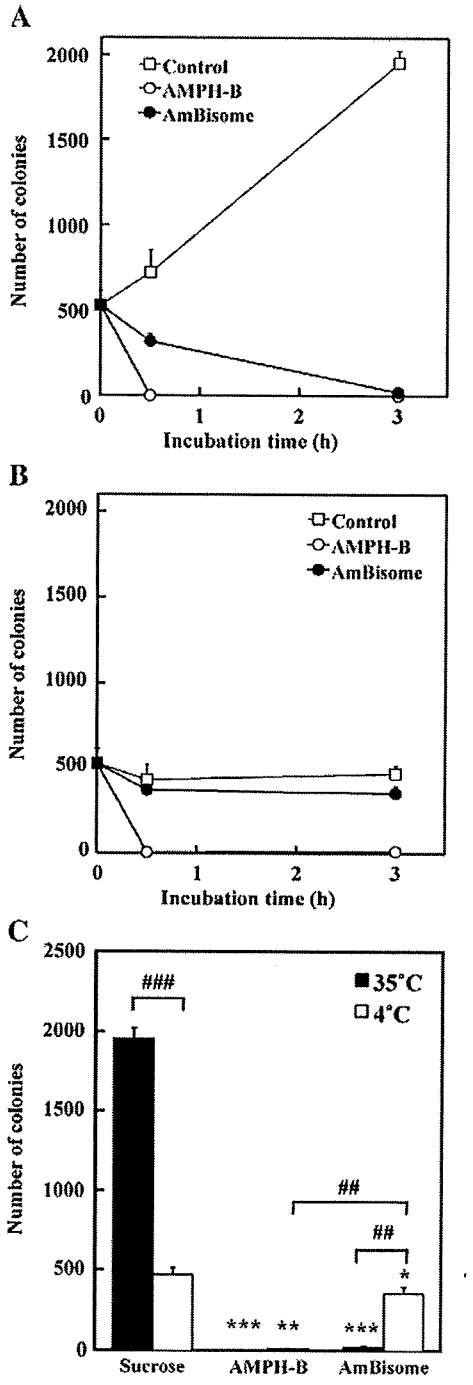


**Fig. 1.** Temperature-dependent antifungal activity of AmBisome against *Saccharomyces cerevisiae*. After the optical density of a *S. cerevisiae* suspension was adjusted to 0.1, sucrose, AMPH-B, or AmBisome (20 μM as AMPH-B) was added to the yeast cell suspension; and incubation was carried out at 35 °C (A) or 4 °C (B) for 0.5 or 3 h in MOPS-buffered RPMI 1640 medium. After the cells had been washed with PBS, they were plated on YPD/agar medium. After 24 h of incubation at 30 °C, the number of colonies formed was counted. The difference in activity between temperatures is also summarized (C). Significant differences are shown (* $P<0.05$, ** $P<0.01$, *** $P<0.001$ *vs.* Sucrose; ## $P<0.01$, ### $P<0.001$ as indicated by the brackets).

### 3.4. Disruption of AmBisome at the yeast cell surface

It is not clear whether or not the disruption of AmBisome is a prerequisite for AMPH-B release from the liposomal membrane after

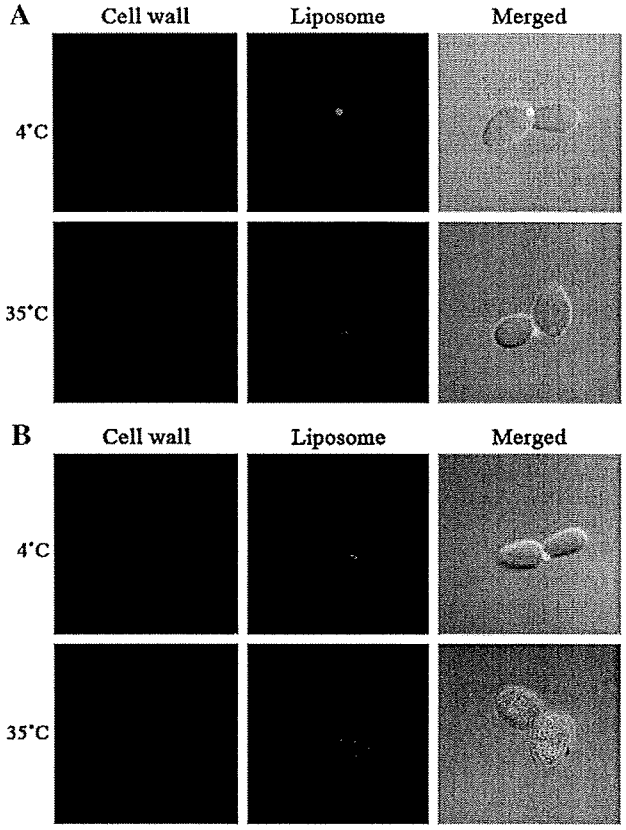


**Fig. 2.** Binding of AmBisome to cell wall of yeast cells. NBD-labeled AmBisome was added to yeast cell suspensions that were then incubated in MOPS-buffered RPMI 1640 medium at 4 or 35 °C for 3 h (A) or 24 h (B). Then, the yeast cell wall was stained with Fluorescent Brightener 28, and localization of AmBisome was observed with a confocal laser-scanning microscope. Green and blue images show AmBisome and the cell wall, respectively. Bar indicates 10 μm.

binding of AmBisome to the surface of yeast cells. To clarify this point, we prepared rhodamine-encapsulated AmBisome and investigated the disruption of the liposomes after exposure of the yeast cells to it.

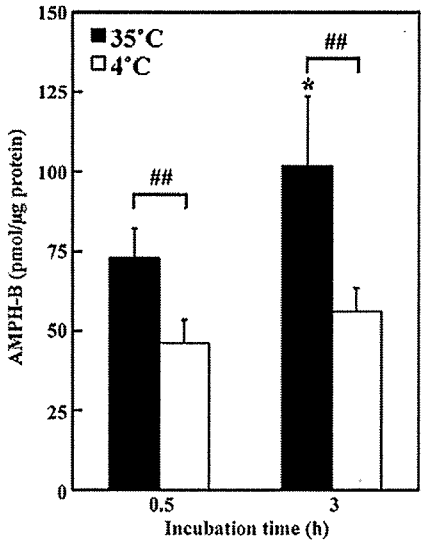


**Fig. 3.** Temperature-dependent transfer of AMPH-B to yeast cells. AmBisome was added to cell suspensions of *Saccharomyces cerevisiae* that were then incubated in MOPS-buffered RPMI 1640 medium at 4 or 35 °C for 0.5 or 3 h. After the cells had been washed with PBS, the amount of AMPH-B in the yeast cells was measured by HPLC. Significant differences are indicated (* $P<0.05$ *vs.* 35 °C; ## $P<0.01$, as indicated by the brackets).

When rhodamine-encapsulated AmBisome was incubated with yeast cells at a low density or number at 35 °C, the fluorescence of rhodamine released from AmBisome was very little, and most of the fluorescence was detected in the liposome fraction (Fig. 4A). A similar result was obtained even when the number of yeast cells was increased. Furthermore, there was no apparent difference in liposomal disruption between at 4 and 35 °C incubation (Fig. 4B). These results suggest that AmBisome was not disrupted at least until 3 h after binding to the cell surface and that AmBisome-derived AMPH-B was transferred to the fungal cell membrane without liposomal disruption.

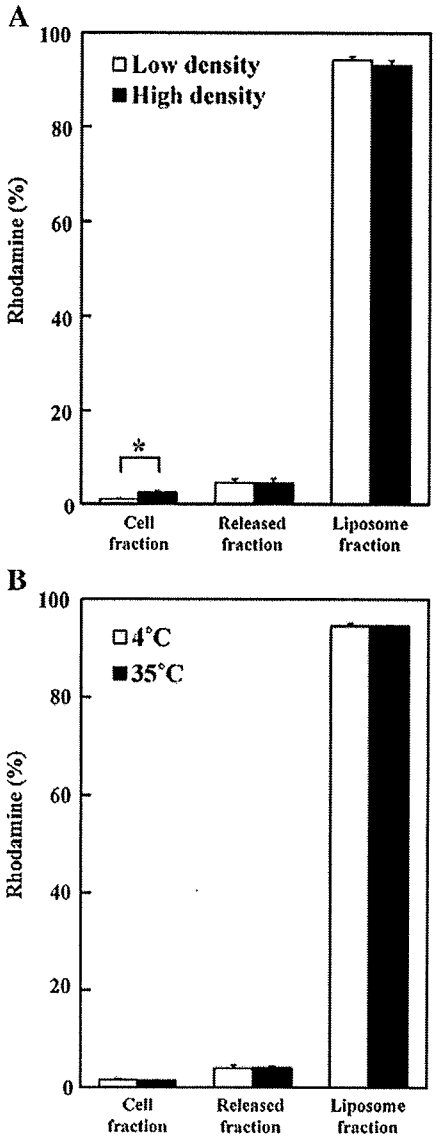


**Fig. 4.** Investigation of liposomal disruption during exposure of yeast cells to AmBisome. Rhodamine-encapsulating AmBisome was added to a suspension of *Saccharomyces cerevisiae* that had been adjusted to a low ($OD_{600}=0.1$) or high ($OD_{600}=0.3$) density, and the cells were then incubated in MOPS-buffered RPMI 1640 medium at 35 °C for 3 h (A). The culture medium was collected and ultracentrifuged to remove intact AmBisome. The fluorescence intensity of the rhodamine that had been released from rhodamine-encapsulating AmBisome into the medium was measured in the supernatant. Disruption of AmBisome at 4 °C was also examined (B). Asterisk shows a significant difference between bracketed values (* $P<0.05$).

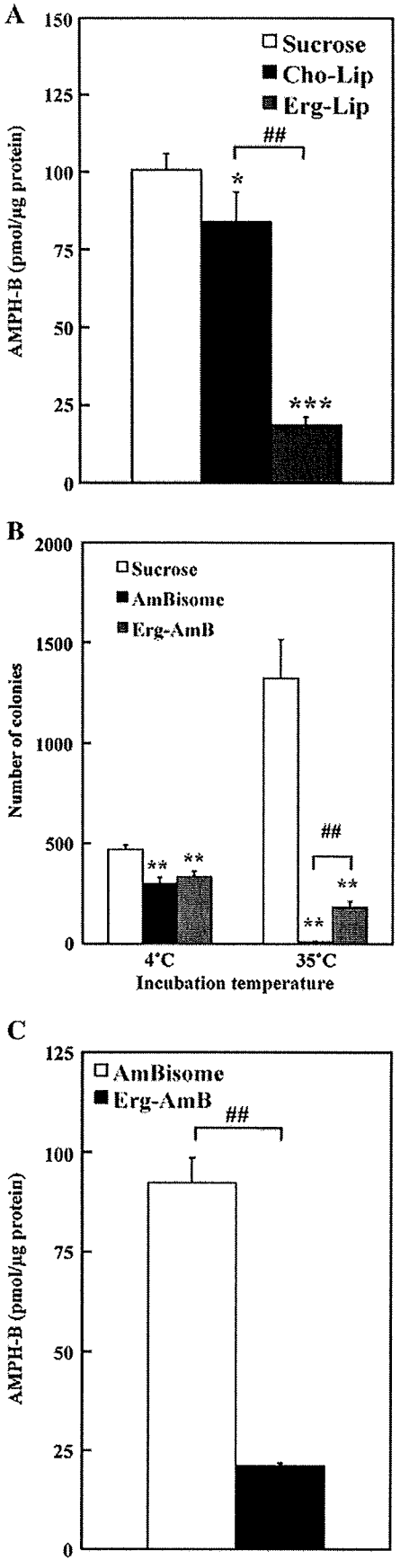


### 3.5. Importance of differential AMPH-B affinity for AmBisome and yeast cell membrane

To examine the importance of AMPH-B affinity for the fungal cell membrane during the transfer of AmBisome-derived AMPH-B to the membrane, we examined the transfer of AMPH-B to yeast cells in the presence of cholesterol liposomes (Cho-Lip) or ergosterol liposomes (Erg-Lip) in which AMPH-B was not entrapped. As a result, the transfer of AMPH-B from AmBisome was significantly reduced in the presence of Erg-Lip, whereas little inhibition was observed in the presence of Cho-Lip (Fig. 5A), confirming that the affinity of AMPH-B for ergosterol-containing membrane is stronger than that for cholesterol-containing one.

Next, we prepared liposomal AMPH-B containing ergosterol (Erg-AmB) instead of cholesterol and examined the antifungal activity of Erg-AmB against yeast cells. At 4 °C, the antifungal activity of Erg-AmB was attenuated just as in the case of AmBisome (Fig. 5B). However, at 35 °C Erg-AmB failed to kill all of the yeast cells whereas AmBisome completely destroyed them at this temperature (Fig. 5B). Furthermore, when the transfer of AMPH-B from Erg-AmB to the cells was investigated, the amount of AMPH-B in the cells was reduced after 3 h of incubation (Fig. 5C). These results indicate that ergosterol in the liposomes controlled the antifungal effect of liposomal AMPH-B and that the different affinity of AMPH-B for cholesterol and ergosterol played an important role in the transfer of AMPH-B to the fungal cell membrane.

### 3.6. Importance of liposomal membrane fluidity in temperature-dependent antifungal activity of AmBisome

Since the transfer of AMPH-B from AmBisome to the fungal cell membrane was dependent on the incubation temperature, we hypothesized that liposome membrane fluidity was a key factor in the transfer of AMPH-B. To examine the importance of membrane fluidity on the transfer of AMPH-B from AmBisome, we prepared AMPH-B liposomes composed of the highly fluid phospholipids EPC and EPG (Egg-AmB) instead of HSPC and DPPG. To measure the membrane fluidity of both liposomes, fluorescence recovery after photobleaching (FRAP) experiment was performed. NBD-labeled both liposomes were prepared, and FRAP measurement was recorded by using confocal laser scanning microscope (LSM510META). As a result, the fluorescence of NBD-PE in NBD-labeled Egg-AmB was recovered to more than 80% at 50 s after photobleaching and the diffusion coefficient was $8.2 \times 10^{-2} \mu m^2/s$, whereas the recovery of fluorescence in NBD-labeled AmBisome was little observed. This result indicates that liposome membrane fluidity of Egg-AmB is far higher than that of AmBisome. Then, the antifungal effect of Egg-AmB against *S. cerevisiae* was investigated at 4 or 35 °C incubation. Egg-AmB not only completely damaged yeast cells at 35 °C, but also showed the antifungal effect at 4 °C to some extent (Fig. 6A). When localization of NBD-labeled Egg-AmB in the yeast cells was observed under the confocal laser-scanning microscope, the fluorescence of Egg-AmB was present in the cytoplasm at both 4 and 35 °C after a 3-h incubation (Fig. 6B), whereas similar images were observed only after a 24-h incubation with AmBisome at 35 °C (Fig. 2B). Furthermore, the increase in the amount

**Fig. 5.** Effect of ergosterol on antifungal activity of AmBisome. AmBisome was added to yeast cell suspensions of *Saccharomyces cerevisiae* that were then incubated in the absence or presence of drug-free cholesterol liposome (Cho-Lip) or drug-free ergosterol liposome (Erg-Lip) for 3 h at 35 °C in MOPS-buffered RPMI 1640 medium. Then, the amount of AMPH-B in the cells was measured (A). Yeast cells were also incubated with sucrose, AmBisome or liposomal AMPH-B containing ergosterol (Erg-AmB) at 4 or 35 °C for 3 h. After the cells had been washed with PBS, they were plated on YPD/agar medium. After a 24-h incubation at 30 °C, the number of formed colonies was counted (B). The amount of AMPH-B in yeast cells after 3 h of incubation at 35 °C was also measured (C). Significant differences are shown (* $P<0.05$, ** $P<0.01$, *** $P<0.001$ *vs.* Sucrose; ## $P<0.01$, as indicated by the bracket).

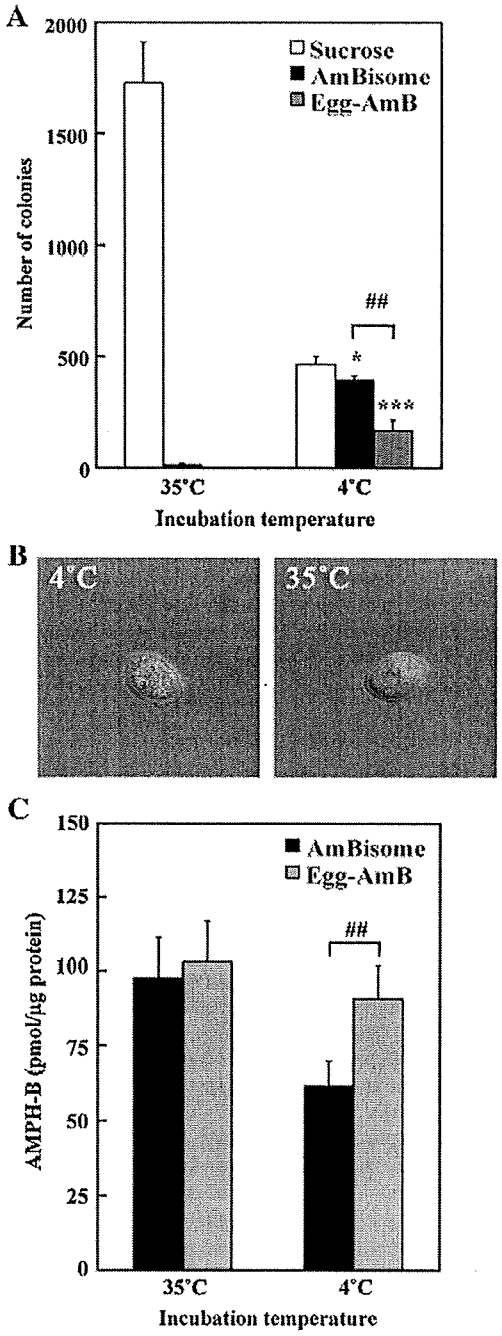


**Fig. 6.** Effect of liposome-membrane fluidity on antifungal activity of AmBisome. Cell suspensions of *Saccharomyces cerevisiae* were incubated with sucrose, AmBisome or liposomal AMPH-B composed of EPC and EPG (Egg-AmB) at 4 or 35 °C for 3 h in MOPS-buffered RPMI 1640 medium. After the cells had been washed with PBS, they were plated on YPD/agar medium. After 24 h of incubation at 30 °C, the number of colonies formed was counted (A). Localization of NBD-labeled Egg-AmB after a 3-h incubation at 4 or 35 °C was observed (B) and the amount of AMPH-B in the yeast cells after 3 h of incubation at 4 or 35 °C was also measured (C). Significant differences are shown (* $P<0.05$, *** $P<0.001$ vs. Sucrose; ## $P<0.01$, as indicated by the bracket).

of AMPH-B transferred from Egg-AmB to the cells after the 4 °C incubation was obvious (Fig. 6C). These results suggest that liposomal membrane fluidity was involved in the transfer of AMPH-B from AmBisome to the fungal cell membrane and indicate that AMPH-B in fluid liposomes would be easier to transfer to other membranes with high affinity for AMPH-B.

## 4. Discussion

It is known that liposomalization or polymerization of a drug often enables enhancement of the therapeutic effects and reduces the side effects by improving the pharmacokinetics and pharmacodynamics of the original drug in the body [15,16]. The liposomal antifungal drug AmBisome is a representative example of a liposome that incorporates AMPH-B in its membrane, enhances the stability of AMPH-B in the bloodstream and reduces the side effects of the drug [9,10]. AmBisome shows a potent antifungal effect against fungal cells such as *Candida albicans*, *Cryptococcus neoformans*, and *Aspergillus fumigatus*, resulting in the successful treatment of deep mycosis caused by them [17,18]. AmBisome exerts its effect by the binding of AMPH-B from AmBisome to ergosterol in the fungal cell membrane, which binding enhances the permeability of the fungal cell membrane and promotes the leakage of cellular substances and subsequent fungal cell death [3,19]. Thus, the transfer of AMPH-B from AmBisome to the fungal cell membrane is a key step for AmBisome to manifest its antifungal activity. In the case of other liposomal drugs, the release of the encapsulated drug from the liposome is critical for drug activity. For example, liposomal doxorubicin shows a potent cytotoxic effect against various kinds of cancer. The action mechanism of liposomal doxorubicin is considered to be as follows: Liposomal doxorubicin is incorporated into the cells by the endocytic pathway, the liposome is disrupted in lysosomes, and the encapsulated doxorubicin is released and transferred to nuclei to damage the cell. On the other hand, it is expected that the action mechanism of AmBisome against fungal cells would be different from that of other liposomal drugs against mammalian cells, since fungal cells possess a protective cell wall around their cell membrane, unlike mammalian cells [20]. In fact, it has not been fully clarified whether AmBisome can pass through the cell wall or not. In the present study, we aimed at elucidating the action mechanism of AmBisome, especially the mechanism of the transfer of AMPH-B from the liposome to ergosterol in the fungal cell membrane.

We firstly focused on the temperature dependence of AmBisome activity by comparing the antifungal effect of AmBisome against *S. cerevisiae* at 4 and 35 °C. As a result, AmBisome showed strong time-dependent antifungal activity at 35 °C, whereas free AMPH-B eradicated the yeast cells completely after just a 0.5-h incubation (Fig. 1A), indicating that AmBisome required a certain period of time to show its antifungal activity compared with AMPH-B. Furthermore, AmBisome did not show the activity at 4 °C, whereas AMPH-B showed strong activity at this same temperature (Fig. 1B, C). These results suggest that antifungal activity of AmBisome is dependent on the release and transfer of its AMPH-B to the fungal cell membrane. This temperature-dependent AmBisome activity would not be due to a difference in the localization of AmBisome in yeast cells, since AmBisome bound to yeast cells similarly at both 4 and 35 °C (Fig. 2A). Similar binding of AmBisome at 4 and 35 °C was also observed after a 0.5-h incubation (data not shown). These data also support the idea that the release and transfer of AMPH-B from AmBisome is critical for the antifungal efficacy instead of a temperature-dependent amount of AmBisome binding. In fact, the amount of AMPH-B transferred from AmBisome increased in a temperature-dependent manner (Fig. 3).

Adler-Moore et al. previously reported that gold-labeled AmBisome binds to the fungal cell wall, as observed by electron microscopy [13]. In our study, AmBisome actually bound to the cell wall and was topically observed to become localized at the budding or interface site of *S. cerevisiae* after a 3-h incubation at either 4 or 35 °C (Fig. 2A). In their review article Lesage et al. stated that the structure and components of the yeast cell wall change according to cell growth and are especially different during bud emergence and at the mother/daughter interface [21]. Thus, we hypothesize that these regions of the cell wall are susceptible to binding by AmBisome and that its

AMPH-B is transferred to the fungal cell membrane at these regions in a temperature-dependent manner. However, further research will be needed to elucidate whether AmBisome directly interacts with the fungal cell membrane or not.

Furthermore, AmBisome-derived fluorescence was present in the cytoplasm after 24 h of incubation at 35 °C but not at 4 °C (Fig. 2B). We speculate that the fungal cell death causes the entry of AmBisome into the cytoplasm.

We next examined the possible disruption of AmBisome for the transfer of AMPH-B to the fungal cell membrane. As a result, AmBisome-derived rhodamine release was minimal after exposure to the drug, even when the number of yeast cells was increased or the incubation temperature was changed (Fig. 4). These results indicate that the transfer of AMPH-B from AmBisome occurred at least until 3 h after attachment to the outside of fungal cells without disruption of the liposomal architecture of AmBisome.

Finally, to identify the key factor for the transfer of AMPH-B from AmBisome, we prepared liposomal AMPH-B with different lipid compositions and investigated the effect of lipid composition on AmBisome-induced antifungal activity. When AMPH-B was incorporated into liposomes containing ergosterol instead of cholesterol, the antifungal effect against *S. cerevisiae* was significantly reduced compared with that of AmBisome at 35 °C, where the membrane fluidity is considered to be similar (Fig. 5B). In addition, the amount of transferred AMPH-B to the yeast cells from Erg-AmB was decreased (Fig. 5C). It is known that the affinity of AMPH-B for ergosterol is about 10 times higher than that for cholesterol [22]. Thus, this result suggests that liposomal ergosterol prevented the release of AMPH-B from liposomes, the consequence being suppression of the transfer of AMPH-B from AmBisome to the fungal cell surface. A number of studies have been presented about the reason for the high affinity of AMPH-B to ergosterol in comparison with that to choresterol. Recently, Baran et al. suggested that AmB-ergosterol-AmB aggregates simulated of 2:1 stoichiometry retain significantly higher stability and relatively rigid, "sandwich" geometry due to Van der Waals forces and the intermolecular hydrogen bonds [23]. In contrast, cholesterol does not form this sandwich geometry that would be the reason for the low affinity of AMPH-B to cholesterol in comparison with this to ergosterol [23].

On the contrary, when AMPH-B was incorporated into liposomes composed of high-fluidity phospholipids, namely, EPC and EPG, the antifungal effect against *S. cerevisiae* was observed even at 4 °C, where the membrane fluidity is rather low and AmBisome showed little effect (Fig. 6A). In addition, the amount of AMPH-B transferred to the yeast cells from Egg-AmB was increased (Fig. 6C). When localization of NBD-labeled Egg-AmB in the yeast cells was examined, the fluorescence of Egg-AmB was present in the cytoplasm even after 0.5 h of incubation (Fig. 6B). It is known that the phase-transition temperature of EPC and HSPC is about −10 °C and 55 °C, respectively. When the membrane fluidity of Egg-AmB and AmBisome was compared using NBD-PE by FRAP experiment, the membrane fluidity of Egg-AmB is higher than that of AmBisome. According to the result, it is reasonable that the transfer of AMPH-B from Egg-AmB to the fungal cell membrane would occur at the low temperature. Thus, these results suggest that the increased membrane fluidity enhanced the release of AMPH-B from AmBisome and stability of AMPH-B in the liposomal membrane is the key factor for the biological activity of liposomal AMPH-B.

According to the report by Legrand et al., the critical micelle concentration (CMC) of AMPH-B was 0.1 μM in aqueous solution. They showed that the concentration of free AMPH-B released by AmBisome at 1 μg/ml (1.08 μM) was about 0.08 μg/ml (0.09 μM), which was below the CMC of AMPH-B [24]. We investigated the release of AMPH-B from AmBisome at high concentration (2.22 mM) in MOPS-buffered RPMI 1640 medium at room temperature using an ultrafiltration method. As a result, time-dependent release of AMPH-B was not observed (0.293 and 0.369 μM at 0 and 24 h after incubation, respectively; 0.013% and 0.017% of total AMPH-B in AmBisome), suggesting that AmBisome is quite stable, but allows the release of a little amount of AMPH-B (data not shown). Based on such information and results obtained in the present study, we hypothesized that ergosterol in the fungal cell membrane may be able to increase the amount of AMPH-B released from AmBisome or induce the continuous release of AMPH-B from AmBisome without direct interaction to AmBisome after AmBisome attachment to the fungal cell wall.

## 5. Conclusion

Our present study demonstrated that AmBisome bound to the cell wall of yeast cells and that the AMPH-B from AmBisome was transferred to the yeast cell membrane without obvious disruption of the liposome formulation. Furthermore, we demonstrated that the transfer of AMPH-B was dependent on temperature and fluidity of the liposome membrane.

## Acknowledgements

The authors thank all members of the Department of Medical Biochemistry at the University of Shizuoka for their helpful advice in this study.

## Appendix A. Supplementary data

Supplementary data associated with this article can be found, in the online version, at doi:10.1016/j.jconrel.2009.09.019.

## References

[1] M.E. Klepser, E.J. Wolfe, R.N. Jones, C.H. Nightingale, M.A. Pfaller, Antifungal pharmacodynamic characteristics of fluconazole and amphotericin B tested against *Candida albicans*, Antimicrob. Agents Chemother. 41 (6) (1997) 1392–1395.
[2] L. Ostrosky-Zeichner, K.A. Marr, J.H. Rex, S.H. Cohen, Amphotericin B: time for a new "gold standard", Clin. Infect. Dis. 37 (3) (2003) 415–425.
[3] B.E. Cohen, Concentration- and time-dependence of amphotericin-B induced permeability changes across ergosterol-containing liposomes, Biochim. Biophys. Acta 857 (1) (1986) 117–122.
[4] I. Fournier, J. Barwicz, P. Tancrede, The structuring effects of amphotericin B on pure and ergosterol- or cholesterol-containing dipalmitoylphosphatidylcholine bilayers: a differential scanning calorimetry study, Biochim. Biophys. Acta 1373 (1) (1998) 76–86.
[5] K.M. Wasan, G. Lopez-Berestein, The interaction of liposomal amphotericin B and serum lipoproteins within the biological milieu, J. Drug Target 2 (5) (1994) 373–380.
[6] R. Sabra, R.A. Branch, Amphotericin B nephrotoxicity, Drug Saf 5 (2) (1990) 94–108.
[7] I. Bekersky, R.M. Fielding, D.E. Dressler, J.W. Lee, D.N. Buell, T.J. Walsh, Plasma protein binding of amphotericin B and pharmacokinetics of bound versus unbound amphotericin B after administration of intravenous liposomal amphotericin B (AmBisome) and amphotericin B deoxycholate, Antimicrob. Agents Chemother. 46 (3) (2002) 834–840.
[8] J. Adler-Moore, R.T. Proffitt, Effect of tissue penetration on AmBisome efficacy, Curr. Opin. Investig. Drugs 4 (2) (2003) 179–185.
[9] K. Takemoto, Y. Yamamoto, Y. Ueda, Evaluation of antifungal pharmacodynamic characteristics of AmBisome against *Candida albicans*, Microbiol. Immunol. 50 (8) (2006) 579–586.
[10] K. Takemoto, Y. Yamamoto, Y. Ueda, Y. Sumita, K. Yoshida, Y. Niki, Comparative study on the efficacy of AmBisome and Fungizone in a mouse model of pulmonary aspergillosis, J. Antimicrob. Chemother. 57 (4) (2006) 724–731.
[11] E. Briones, C.I. Colino, J.M. Lanao, Delivery systems to increase the selectivity of antibiotics in phagocytic cells, J. Control Release 125 (3) (2008) 210–227.
[12] J. Adler-Moore, AmBisome targeting to fungal infections, Bone Marrow Transplant. 14 (Suppl 5) (1994) S3–7.
[13] J. Adler-Moore, R.T. Proffitt, AmBisome: liposomal formulation, structure, mechanism of action and pre-clinical experience, J. Antimicrob. Chemother 49 (Suppl 1) (2002) 21–30.
[14] V.J. Cid, A. Duran, F. del Rey, M.P. Snyder, C. Nombela, M. Sanchez, Molecular basis of cell integrity and morphogenesis in *Saccharomyces cerevisiae*, Microbiol. Rev. 59 (3) (1995) 345–386.
[15] T.M. Allen, P.R. Cullis, Drug delivery systems: entering the mainstream, Science 303 (5665) (2004) 1818–1822.
[16] G. Gaucher, M.H. Dufresne, V.P. Sant, N. Kang, D. Maysinger, J.C. Leroux, Block copolymer micelles: preparation, characterization and application in drug delivery, J. Control Release 109 (1–3) (2005) 169–188.

[17] J.P. Adler-Moore, S.M. Chiang, A. Satorius, D. Guerra, B. McAndrews, E.J. McManus, R.T. Proffitt, Treatment of murine candidosis and cryptococcosis with a unilamellar liposomal amphotericin B formulation (AmBisome), J. Antimicrob. Chemother 28 (Suppl B) (1991) 63–71.
[18] A.C. Leenders, P. Reiss, P. Portegies, K. Clezy, W.C. Hop, J. Hoy, J.C. Borleffs, T. Allworth, R.H. Kauffmann, P. Jones, F.P. Kroon, H.A. Verbrugh, S. de Marie, Liposomal amphotericin B (AmBisome) compared with amphotericin B both followed by oral fluconazole in the treatment of AIDS-associated cryptococcal meningitis, AIDS 11 (12) (1997) 1463–1471.
[19] M. Baginski, H. Resat, E. Borowski, Comparative molecular dynamics simulations of amphotericin B-cholesterol/ergosterol membrane channels, Biochim. Biophys. Acta 1567 (1–2) (2002) 63–78.
[20] M. Kirkham, R.G. Parton, Clathrin-independent endocytosis: new insights into caveolae and non-caveolar lipid raft carriers, Biochim. Biophys. Acta 1745 (3) (2005) 273–286.
[21] G. Lesage, H. Bussey, Cell wall assembly in *Saccharomyces cerevisiae*, Microbiol. Mol. Biol. Rev. 70 (2) (2006) 317–343.
[22] J.D. Readio, R. Bittman, Equilibrium binding of amphotericin B and its methyl ester and borate complex to sterols, Biochim. Biophys. Acta 685 (2) (1982) 219–224.
[23] M. Baran, E. Borowski, J. Mazerski, Molecular modeling of amphotericin B-ergosterol primary complex in water II, Biophys. Chem. 141 (2–3) (2009) 162–168.
[24] P. Legrand, M. Cheron, L. Leroy, J. Bolard, Release of amphotericin B from delivery systems and its action against fungal and mammalian cells, J. Drug Target 4 (5) (1997) 311–319.

# Preventive Effect of Green Tea Catechins on Experimental Tumor Metastasis in Senescence-Accelerated Mice

Kosuke SHIMIZU,[a] Naomi KINOUCHI SHIMIZU,[a] Wakako HAKAMATA,[a] Keiko UNNO,[b] Tomohiro ASAI,[a] and Naoto OKU*,[a]

[a] *Department of Medical Biochemistry and Global COE Program, University of Shizuoka; and* [b] *Laboratory of Bioorganic Chemistry, School of Pharmaceutical Sciences, University of Shizuoka; 52–1 Yada, Suruga-ku, Shizuoka, Shizuoka 422–8526, Japan.* Received August 27, 2009; accepted October 5, 2009; published online October 29, 2009

**Successful avoidance of the immune surveillance system is critical for the development of a blood–borne metastasis. Previous findings suggest that experimental tumor metastasis was enhanced in senescence-accelerated mice prone 10 (SAMP10) due to a reduction in immune surveillance potential with age. In the present study, water containing green tea (GT)-catechins was freely given to SAMP10 mice, and the chemopreventive effect of GT-catechin intake on tumor metastasis was examined. Natural killer cell activity, which is an indicator of immune surveillance potential and is reduced in control mice with age, was maintained by GT-catechin intake. The early accumulation of lung-metastatic K1735M2 melanoma cells in lungs after intravenous injection of the cells and subsequent experimental lung metastasis was investigated in mice given GT-catechins. The accumulation at 6 and 24 h after injection of K1735M2 cells was significantly suppressed, and the number of lung-metastatic colonies was significantly reduced, in comparison with those in control mice. The results suggest that GT-catechin intake prevented the experimental tumor metastasis in aged SAMP10 mice *via* its inhibition of a reduction in immune surveillance potential with age.**

**Key words** aging; tumor metastasis; green tea catechin; immune surveillance

Tumor metastasis is a key step in the development of a tumor and becomes a critical trigger for the death of a patient. Hematogenous metastasis is established by a series of steps, which begin with the dissociation from primary sites and culminate with the formation of metastatic colonization.[1] This process is greatly dependent on surrounding host factors such as host resistance to cancerous cells.[2,3] In a previous study, we demonstrated that the early accumulation of metastatic tumor cells in a target organ after intravenous injection of the cells and following tumor metastasis were enhanced by reduction of the host immune surveillance potential,[4,5] suggesting that avoidance of the surveillance associated with immune cells, such as natural killer (NK) cells, was a critical step for the completion of an experimental tumor metastasis.

The senescence-accelerated mice prone (SAMP) strain has been established as a mouse model for aging research[6] and exhibits a more accelerated senescence process than normal mice.[7,8] By using this model, we found that the immune surveillance potential of 8-month-old aged SAMP10 mice was lower than that of 2-month-old young mice, and that the experimental lung metastasis was significantly induced in aged mice. These data suggest that the aging process produces an environment susceptible to metastatic tumor cells in the bloodstream to complete metastasis, and that such an environment is produced with age due to the reduced immune surveillance potential.[9]

Green tea (GT)-catechins are functional polyphenols, and are known to have various actions, such as antibiotic, anti-inflammatory, antioxidative, and anti-cancer effects. It is anticipated they will become useful as a functional food that promotes human health and longevity. Although animal studies have shown that GT-catechin treatment suppressed tumorigenesis, tumor growth, and tumor angiogenesis,[10,11] the crucial mechanism of the action of GT-catechin against cancer has not been fully elucidated. Our previous study demonstrated that (−)-epigallocatechin gallate (EGCG, a major component of GT-catechins) suppressed tumor angiogenesis through the inhibition of membrane type-1 matrix metalloproteinase (MT-1MMP) activity and subsequent induction of dormancy of solid tumor growth.[12,13] Tachibana *et al.* also reported that 67-kDa laminin receptors are a receptor for EGCG and that EGCG treatment inhibited the receptor-mediated signaling pathway and subsequent tumor cell growth.[14,15] Several reports have described various such approaches to treat and prevent cancer using GT-catechins. In the present study, we hypothesized that GT-catechin intake modulates the immune surveillance potential in aged mice, and enhances the susceptibility to experimental tumor metastasis. To prove this, we exposed SAMP10 mice to GT-catechin in their drinking water for an extended period of time (aged/catechin mice) and examined their NK activity as an indicator of immune surveillance potential. We then also examined the accumulation of K1735M2 melanoma cells in the lungs, the target organ, after intravenous injection of the cells as well as the preventive effect of GT-catechin intake on experimental tumor metastasis.

## MATERIALS AND METHODS

**Animals** SAMP10 mice were purchased from Japan SLC Inc. (Shizuoka, Japan). They began to show several senescence symptoms such as brain atrophy and dehairing from about 6 months-old. Since their immune surveillance potential was adequately reduced at 8 months-old,[9] we used 8-month-old or older SAMP10 mice as an appropriate model for the cancer prone age (aged SAMP10 mice). In another group of aged mice (aged/catechin SAMP10 mice), water containing 0.02% (w/v) GT-catechins (Polyphenon70S, Mitsui Norin Co., Ltd., Tokyo) was given *ad libitum* beginning

* To whom correspondence should be addressed. e-mail: oku@u-shizuoka-ken.ac.jp

at the age of 1-month-old. Polyphenon70S is a crude extract from green tea and contains various kinds of catechins such as (−)-epigallocatechin gallate (EGCG), which is the main component, and (−)-epicatechin gallate (ECG), (−)-epigallocatechin (EGC), and epicatechin (EC). The contents of the various catechins in Polyphenon70S are shown in Table 1 (Information was provided by Mitsui Norin Co., Ltd.). Animal care and experiments were performed in accordance with the Guidelines for the Care and Use of Laboratory Animals of the University of Shizuoka.

**Cells** Highly lung-metastatic, murine K1735M2 melanoma cells were kindly provided by Dr. Jun Yokota of the National Cancer Center (Tokyo, Japan). These cells were cultured in Dulbecco's modified Eagle's medium (DMEM) containing 10% fetal bovine serum (FBS, Japan Bio Serum Co., Ltd., Hiroshima, Japan) at 37 °C in the presence of 5% $CO_2$ in a humid atmosphere. NK-sensitive YAC-1 cells were purchased from the RIKEN Bioresource Center Cell Bank (Ibaraki, Japan) and cultured in RPMI1640 medium containing 10% FBS at 37 °C in the presence of 5% $CO_2$.

**Experimental Lung Metastatic Model** K1735M2 cells ($5\times10^4$ cells/mouse) were intravenously injected into 2-month-old, 8-month-old, or 13-month-old SAMP10 mice *via* a tail vein and metastatic colonies were allowed to form in their lungs. In the chemoprevention experiment, K1735M2 cells were injected into 8-month-old aged or 8-month-old aged/catechin SAMP10 mice. Twenty-one days after injection of the tumor cells, the animals were sacrificed under diethylether anesthesia, and their perfused lungs were isolated. Tumor metastasis was evaluated by counting the number of metastatic colonies on the surface of the lungs.

**NK Activity Assay** To measure the NK activity, spleen cells were used as effector cells. Spleen of aged or aged/catechin SAMP10 mice was harvested, and the splenocytes were carefully flushed several times with an 18 G needle-tipped syringe and passed through nylon mesh to prepare the single cell suspension. The resultant cells were washed twice after removal of erythrocytes, and the number of cells was adjusted to 1.25, 2.5, and $5\times10^6$ cells/ml. On the other hand, to prepare target cells for $^{51}Cr$ release assay, mouse NK-sensitive lymphoma YAC-1 cells were used. The cells were incubated with $Na_2{}^{51}CrO_4$ solution (GE Healthcare U.K., Ltd., England) for 60 min at 37 °C for $^{51}Cr$-radiolabeling. After removal of free $^{51}Cr$, the number of radiolabeled cells was adjusted to $1\times10^5$ cells/ml. NK activity of aged or aged/catechin SAMP10 mice was measured by $^{51}Cr$ release assay as follows: Both the effector and the target cells were mixed in 96-well-plates and the plates were incubated for 4 h at 37 °C. After centrifugation of the cell suspension, radioactivity in the supernatant was measured with a gamma counter. Spontaneous release and maximum release were determined by adding RPMI medium containing 10% FBS or 0.1% TritonX-100 solution to the target cell suspension. Specific cytotoxicity of NK cells was determined using the following formula:

$$\%\ \text{lysis} = \frac{(\text{experimental release} - \text{spontaneous release})}{(\text{maximum release} - \text{spontaneous release})} \times 100$$

**Distribution of Metastatic Tumor Cells** K1735M2 cells were radiolabeled with 5-[$^{125}$I]iodo-2′-deoxyuridine ([$^{125}$I]IUdR, GE Healthcare U.K., Ltd.) as described previously.[16] Briefly, these cells were incubated overnight with [$^{125}$I]IUdR at 37 °C in the presence of 5% $CO_2$. After incubation, the cells were collected and centrifuged to remove unincorporated [$^{125}$I]IUdR, and the number of cells was adjusted to $1\times10^4$ cells/mouse for injection. These cells were intravenously injected into 8-month-old aged and 8-month-old aged/catechin SAMP10 mice. At 6 and 24 h after the injection, the mice were sacrificed under anesthesia with diethylether to collect blood and organ (heart, lung, liver, spleen, and kidney) samples. The amount of accumulation of tumor cells in each organ was determined by radioactivity. Distribution data are presented as % injected dose per tissue. The total weight of blood was assumed to be 7.56% of the body weight.

Table 1. Composition of Green Tea Catechins

| GT-catechins | Content (w/w, %) |
|---|---|
| Epigallocatechin (EGC) | 16.5 |
| Epicatechin (EC) | 5.7 |
| Epigallocatechin gallate (EGCG) | 34.5 |
| Epicatechin gallate (ECG) | 10.1 |
| Gallocatechin gallate (GCG) | 2.9 |
| Catechin gallate (CG) | 0.6 |

Information of the content was provided from Mitsui Norin Co., Ltd.

**Statistic Analysis** The variance in a group was evaluated using the *F*-test, and the differences among each group were evaluated using Student's *t*-test.

## RESULTS

**Enhanced Experimental Tumor Metastasis with Age in SAMP10 Mice** We first investigated whether this enhancement of tumor metastasis is dependent on the degree of aging or not. Therefore, 2-month-old, 8-month-old, and 13-month-old SAMP10 mice were prepared and an experimental tumor metastasis assay was performed using K1735M2 melanoma cells. As in a previous report, the number of metastatic colonies in the lungs of 8-month-old aged mice was larger than that in 2-month-old young mice. In 13-month-old aged SAMP10 mice, the number of colonies was further increased (Fig. 1). This result suggested that the susceptibility to experimental tumor metastasis in SAMP10 mice increased in an age-dependent manner.

**Effect of GT-Catechin Intake on NK Activity in Aged SAMP10 Mice** We assumed that GT-catechin intake could suppress the reduction of immune surveillance potential with aging. Two groups of SAMP10 mice were grown in the same environment except that aged/catechin SAMP10 mice were given water containing 0.02% Polyphenon70S instead of normal water beginning at 1-month-old. When these mice reached 8 months-old, their NK activity was examined. The results of $^{51}Cr$ release assay showed that NK activity in aged/catechin SAMP10 mice was significantly higher than that of aged SAMP10 mice for every effector cells/target cells (E/T) ratio (Fig. 2), suggesting that GT-catechin intake suppressed the attenuation of immune surveillance potential with age.

**Suppression of Tumor Cell Accumulation in Lung by GT-Catechin Intake** We next confirmed the early accumulation of lung-metastatic K1735M2 cells after intravenous in-

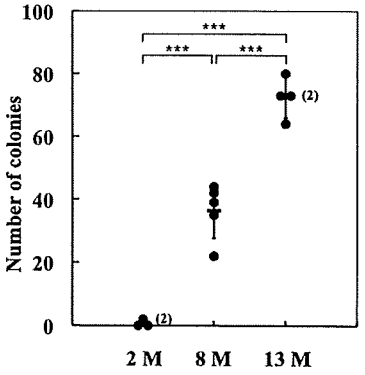


Fig. 1. Age-Dependent Increase in Experimental Tumor Metastasis in SAMP10 Mice

K1735M2 cells ($5\times10^4$ cells/mouse) were intravenously injected into 2-month-old ($n$=4), 8-month-old ($n$=5), and 13-month-old SAMP10 mice ($n$=4), and the number of metastatic colonies in the lungs was counted on day 21 after the tumor cell implantation. The circles in the graph show the number of colonies in individual mice and black bars show the average number of colonies in each mouse. Asterisks indicate the significant differences (***$p$<0.001). Similar results were obtained in a separate experiment.

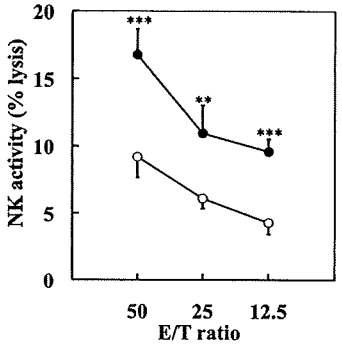


Fig. 2. Recovery of NK Activity by GT-Catechin Intake in Aged SAMP10 Mice

Cytotoxicity of NK cells from the spleen (E: effector cells) of aged (○) and aged/catechin (●) SAMP10 mice against $^{51}$Cr-labeled YAC-1 target cells (T: target cells) was examined as described in Materials and Methods. The radioactivity detected in supernatant medium was measured by a gamma counter, and the NK activity was determined. Significant differences from aged control mice are indicated (**$p$< 0.01; ***$p$<0.001). Similar results were obtained in a separate experiment.

jection in aged and aged/catechin SAMP10 mice, since GT-catechin intake suppressed the reduction in immune surveil-[illegible]otential with age. As shown in Fig. 3A, the accumula-[illegible][$^{125}$I]IUdR-labeled K1735M2 cells in the lungs of [illegible]d/catechin mice was lower than that in aged SAMP10 mice at 6 h after the intravenous injection of the cells. Furthermore, this difference in the accumulation was maintained up to 24 h (Fig. 3B). These results supported the idea that GT-catechin intake suppresses the attenuation of immune surveillance potential, and therefore the clearance of metastatic tumor cells from the target organ is not impaired.

**Preventive Effect of GT-Catechin Intake on Experimental Lung Metastasis in Aged SAMP10 Mice** To investigate the preventive effect of GT-catechin intake on experimental tumor metastasis in old age, lung-metastatic K1735M2 tumor cells ($5\times10^5$ cells/mouse) were injected into the bloodstream of 8-month-old aged, or aged/catechin SAMP10 mice, and then the number of lung-metastatic colonies was determined on day 21 after injection. The number of metastatic colonies in the lung of aged/catechin SAMP10 mice was far less than that in aged SAMP10 mice given normal water (Fig. 4).

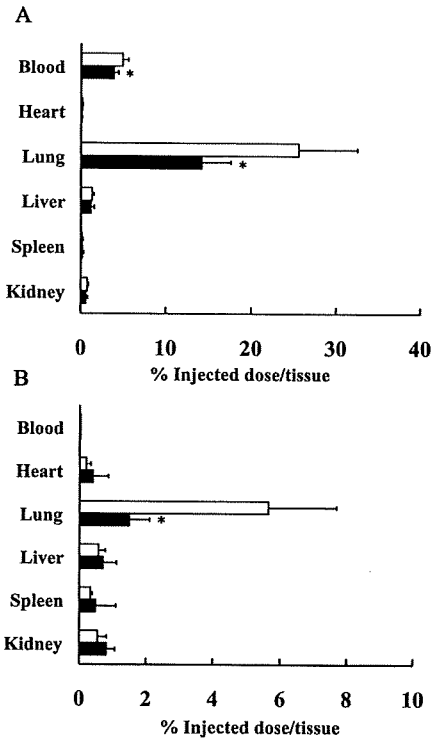


Fig. 3. Distribution of [$^{125}$I]IUdR-Labeled K1735M2 Melanoma Cells in SAMP10

[$^{125}$I]IUdR-labeled K1735M2 melanoma cells ($1\times10^4$ cells/mouse) were injected into aged (open column) and aged/catechin (closed column) SAMP10 mice. The columns indicate the percent accumulation of [$^{125}$I]IUdR-labeled K1735M2 melanoma cells 6 (A) and 24 (B) h after injection. Significant differences from aged mice are indicated (*$p$<0.05). Distribution experiments were performed in two more separate experiments, and similar results were obtained.

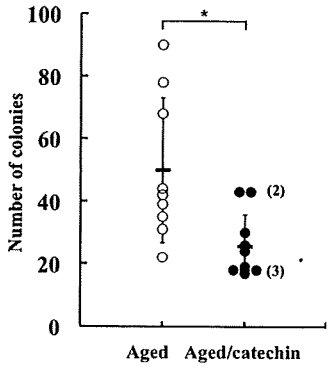


Fig. 4. Preventive Effect of GT-Catechin Intake of Experimental Tumor Metastasis in Aged SAMP10 Mice

K1735M2 cells ($5\times10^4$ cells/mouse) were intravenously injected into aged ($n$=9) and aged/catechin SAMP10 mice ($n$=10) and the metastatic colonies in the lungs were counted on day 21 after tumor implantation. The circles in the graph show the number of colonies in individual mice and black bars show the average number of colonies in each mouse. Asterisks indicate significant differences (*$p$<0.05). Similar results were obtained in a separate experiment.

## DISCUSSION

Senescence is accompanied by various changes in the body, and the internal environment in aged people is different from that in young people. Young people are able to maintain

body homeostasis, and their capacity to defend against foreign substances such as exogenous antigens is superior to that of aged people. Although the mechanism of aging is quite complicated, the accumulation of reactive oxygen species (ROS) in the body is considered to be an important factor in aging.[17] While the relationship between ROS production and cancer development has already been demonstrated, cancer usually starts to develop in middle age or later, suggesting that the aging process is involved in cancer development.[18,19] Our previous study demonstrated that the aging process caused the enhancement of susceptibility to experimental tumor metastasis in senescence-accelerated mice and the reason why it occurs was suggested to be due to a reduction in immune surveillance potential against metastatic tumor cells with age.[9] These findings suggest that the maintenance of a healthy internal environment in aged animals would improve the age-related weakening of the protective effect against experimental metastasis.

To maintain body homeostasis in a favorable condition, a number of functional components have been developed, of which GT-catechin is a well-known example.[20] Many researchers have studied GT-catechin functions and the multifunctional effects of GT-catechins against cancer have been demonstrated.[11] Young animals have been widely used in these basic studies on cancer prevention since it takes a long time to prepare aged animals. It is uncertain, however, whether this situation reflects aged humans, who have high cancer rates, and if these functional components are truly effective at preventing cancer. In the present study, we used SAMP mice as a model to investigate the preventive effect of GT-catechin intake against tumor metastasis in old age.

We first prepared SAMP10 mice of different ages and examined the difference in blood–borne metastasis after intravenous injection of K1735 melanoma cells with age. As shown in Fig. 1, the number of metastatic colonies increased with age. This result confirmed those of our previous study and demonstrated that tumor metastasis was accelerated in an age-dependent manner.[9] In an attempt to inhibit tumor metastasis in old age, we exposed aged SAMP10 mice to GT-catechin water (0.02% Polyphenon70S) for an extended period of time. When the daily intake volume of GT-catechin water was measured, the volume was about 10 ml/d/mouse and was almost the same as for the group given normal water.

At first, the cytotoxicity of splenocytes derived from aged and aged/catechin mice against NK-sensitive YAC-1 cells was measured as an indicator of immune surveillance potential, since the spleen possesses a lot of immune-related cells such as NK cells and plays a critical role in the systemic immune system. GT-catechin intake enhanced the NK activity of aged SAMP10 mice (Fig. 2). Since aging is thought to involve the accumulation of oxidative stress,[21,22] it is possible that an age-dependent burden of oxidative stress causes degradation of the immune defense system against the tumor cells. In actual fact, the cytotoxicity of NK cells is known to be dependent on oxidative stress and the activity is often reduced by ROS.[23] Ferrández *et al.* previously demonstrated that an age-dependent reduction in NK activity was improved by the existence of antioxidant agents such as ascorbic acid and $\alpha$-tocopherol.[24] This result suggests that the antioxidant agents up-regulated NK activity through their protection against ROS. On the other hand, GT-catechins, especially EGCG, are known to work as potent radical scavengers and show antioxidative effects against various types of oxidative stress.[22,25] Unno *et al.* demonstrated that long-term intake of EGCG water up-regulated the level of antioxidative activity in the serum of aged SAMP10 mice.[26] Thus, we speculated that GT-catechin intake provided protection from the accumulation of oxidative stress and improved the reduced NK activity with age. We also reported that consumption of GT-catechin prevented the decline of glutathione peroxidase activity and provided protection from oxidative damage of protein in mouse brain of aged SAMP10.[27] This result also supports our present speculation that GT-catechin intake up-regulates the age-induced reduction in NK activity and has the effect in aged animals.

We next evaluated the effect of GT-catechin intake on blood–borne metastasis induced by intravenous injection of tumor cells. We previously demonstrated that defense against metastatic tumor cells by the immune surveillance system was observed in the early stage of tumor metastasis by use of positron emission tomography (PET).[4,5] In the study, we examined the relationship among the real-time trafficking of lung-metastatic B16BL6 cells, metastatic potential, and the number of the cells injected. When $1\times10^4$ cells were injected, the accumulation of the cells in the lung was less than one-tenth of that obtained with a $1\times10^5$ cell-injection. Metastasis was observed when $1\times10^5$ cells were injected, but not when $1\times10^4$ cells were injected. To clarify the roles of the immune defense system at the initial phase of metastasis, mice were treated with 2-chloroadenosine prior to the tumor cell challenge. As a result, this treatment suppressed not only metastasis but also the early accumulation of the cells in lungs. These results suggest that the immune surveillance, whose action was obvious at the low dose of challenged tumor cells, functions strongly at the initial phase but not at the advanced stages of the metastatic process.[5] Therefore, in the present study, we examined the biodistribution of [$^{125}$I]-labeled K1735M2 cells after intravenous injection and found that early accumulation of tumor cells in their metastatic site was reduced in aged/catechin SAMP10 mice, and this status was also observed at 24 h after injection (Fig. 3).

NK cells are one type of immune cell related to innate immunity, especially immune surveillance, and together with macrophages form the first lines of defense against exogenous agents and tumor cells. Therefore, this result suggested that suppressing the decrease in NK activity with age by GT-catechin intake suppressed the age-induced accumulation of tumor cells in the target organ at the early stage. Experimental tumor metastasis in aged SAMP10 mice was also suppressed by GT-catechin intake (Fig. 4). Shimizu *et al.* reported that daily intake of green tea extract protected against metachronous colorectal adenomas after surgical removal of primary tumors in a pilot study in humans.[28] Our results in the present study may partly explain their finding.

In conclusion, the results of the present study indicate that GT-catechin intake improved the reduction in immune surveillance potential, such as NK activity with age, and suppressed the age-related increase in the susceptibility to experimental tumor metastasis in SAMP10 mice. Thus, daily intake of green tea may provide protection against the weakening of immune surveillance activity with age and thus con-